PMT 5927
aula 2

Capítulos 2.3 a 2.8 do review do DebRoy

2020

2.3. Características das fontes de calor

- 3 fontes de calor: laser, feixe de eletrons ou arco de plasma
- Electron beams and laser beams can deliver either a uniform, pulsed, or otherwise modulated power distribution over time.
- energy absorption by the feedstock materials affects the temperature profiles, deposit geometry, solidification, microstructure and properties of the part.
- Energy absorption depends on the heat source characteristics.
- For lasers, electron beams and plasma arcs the radius and the power density distribution are important properties of the heat source.

- A distribuição de potência do laser deve seguir um perfil gaussiano axisimétrico

$$P_d = \frac{fP}{\pi r_b^2} \exp\left(-f\frac{r^2}{r_b^2}\right)$$

- onde f é o fator de distribuição,
- P é a potência total da fonte
- rb é o raio da fonte de calor
- R é a distância radial a partir do eixo.

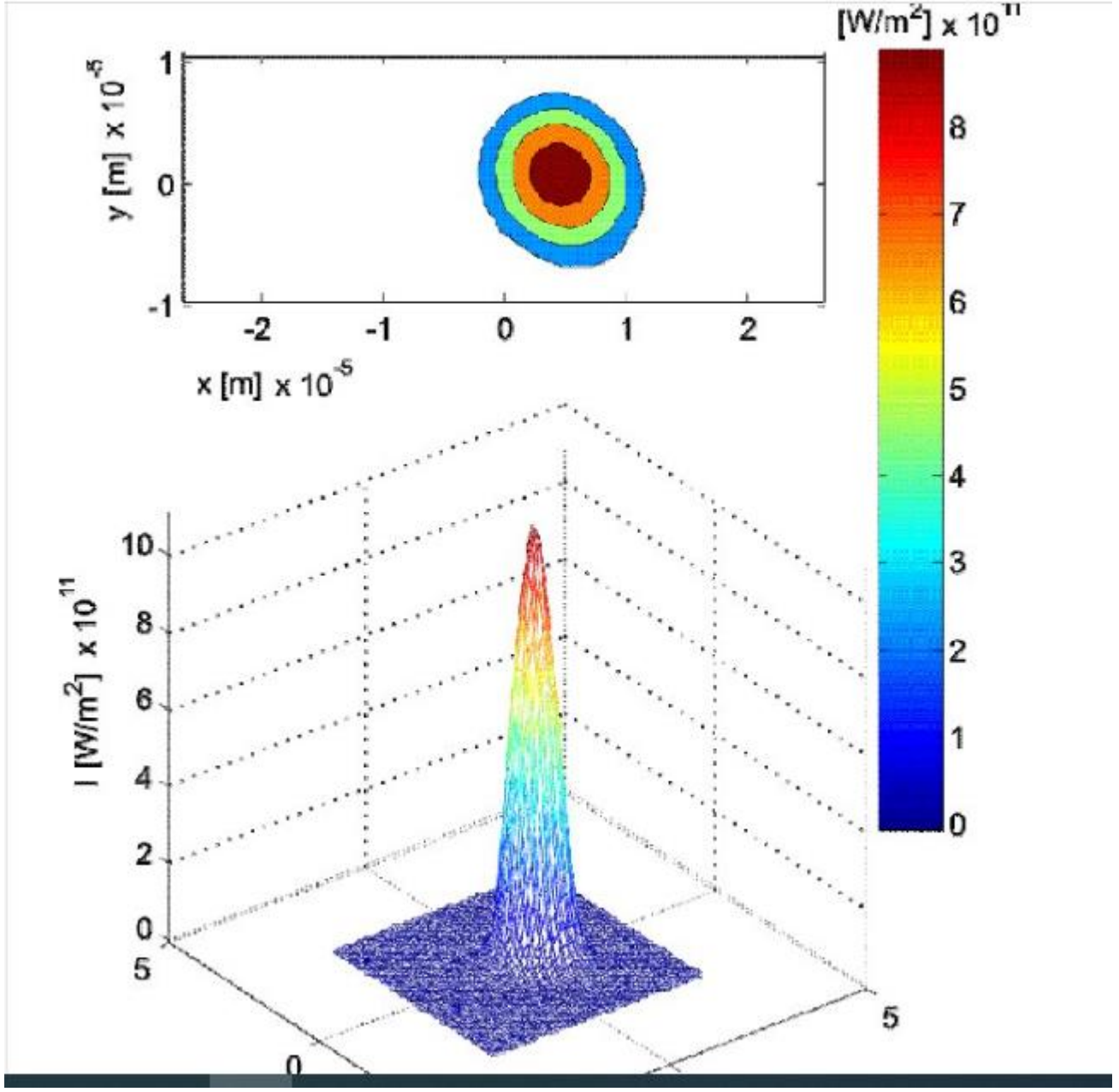

Medida da distribuição de potência do laser

- Por meio de um tubo giratório, com pequenos furos na lateral, o feixe de luz é amostrado em diferentes posições em torno de seu eixo. Através de lentes, esse fragmento de feixe é projetado numa matriz de capacitores (a região fotoativa de um CCD) e faz com que cada capacitor acumule uma carga elétrica proporcional à intensidade da luz incidente naquela localização.
- Com isso, é possível determinar o **spotsize**.

Spot size

- A energia do laser é máxima no centro, e decai numa distribuição normal
- Spotsize (W_0) é o nome que se dá à distância radial entre o eixo do feixe e a posição em que a intensidade decai a E_{max}/e^2
- Chama-se de "diâmetro do feixe" o dobro do spot size.

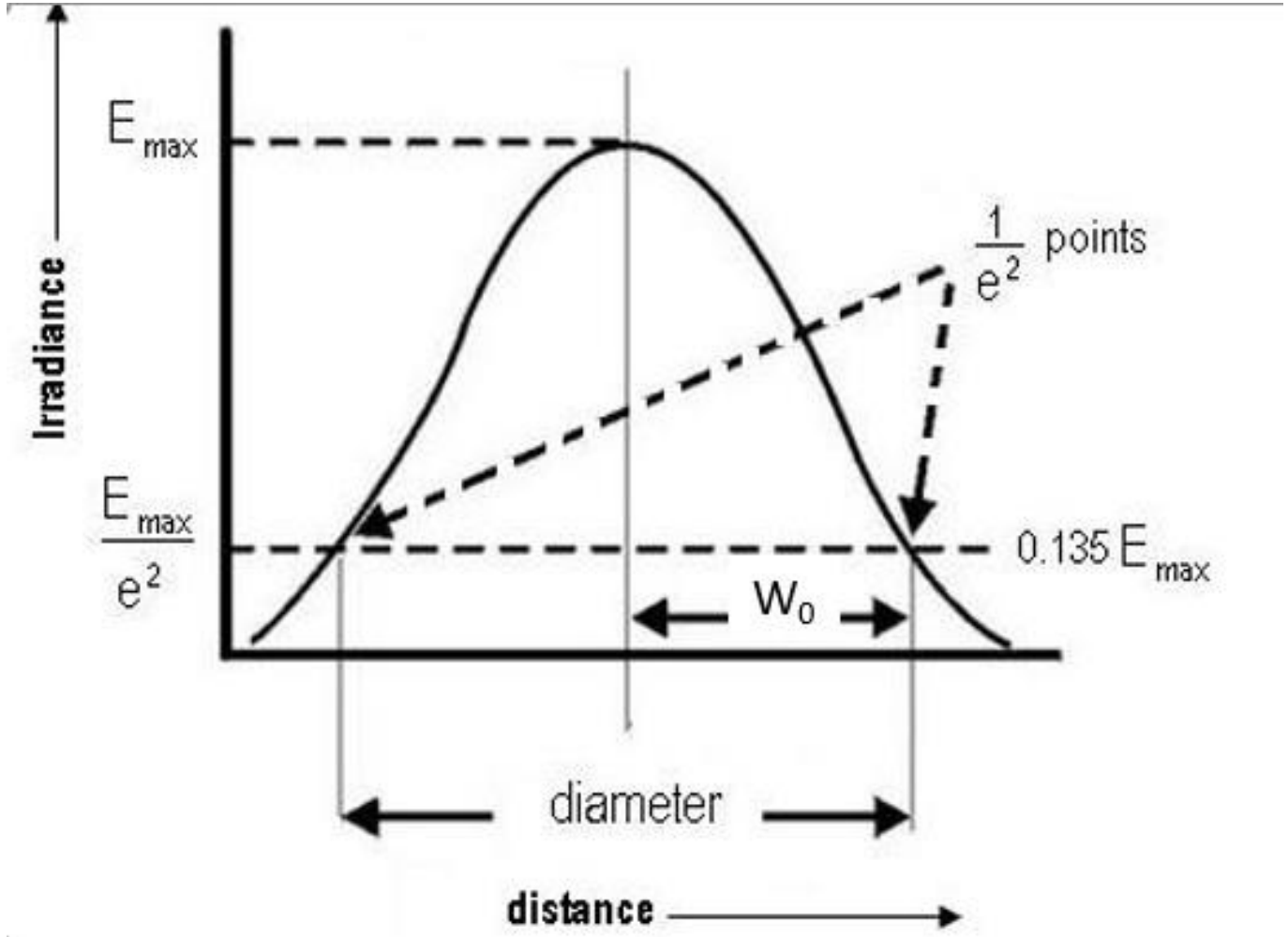

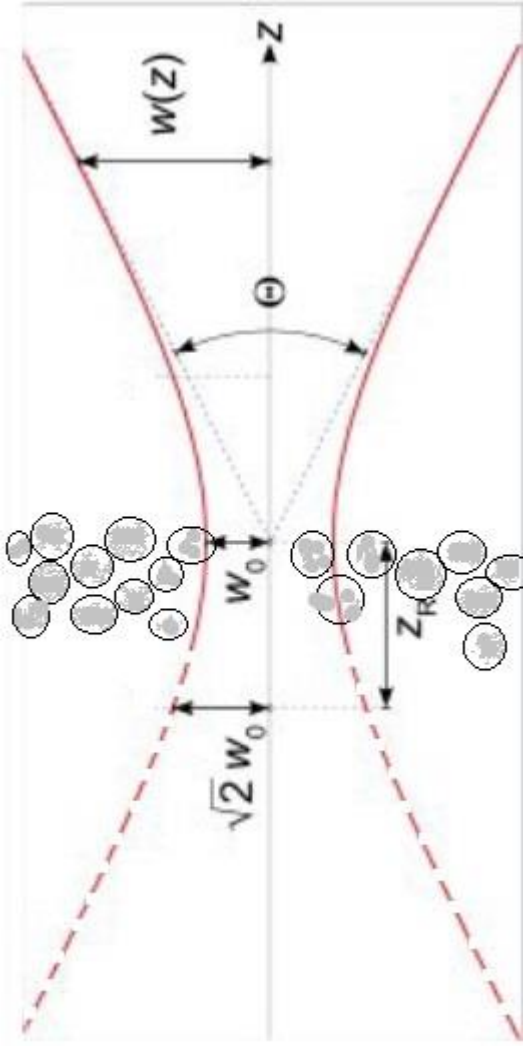

O foco do laser

A lente cria uma convergência do feixe
A convergência não é num ponto , é numa região.
No ponto de máxima convergência, o feixe tem raio W_o
W_o é **o spot size**, é o **raio da área do feixe no ponto focal**, W_o
W_o é da ordem de 50 µm
A zona de convergência tem um comprimento grande,
Define-se o comprimento de Rayleigh Z_R , da ordem de 1 mm
Z_R é a distância entre o ponto de máxima convergência (W=Wo)
e o ponto em que o raio do feixe abriria para W= $\sqrt{2}\,w_0$

Imagem adaptada de material disponível no site da Renishaw

Ângulo do feixe

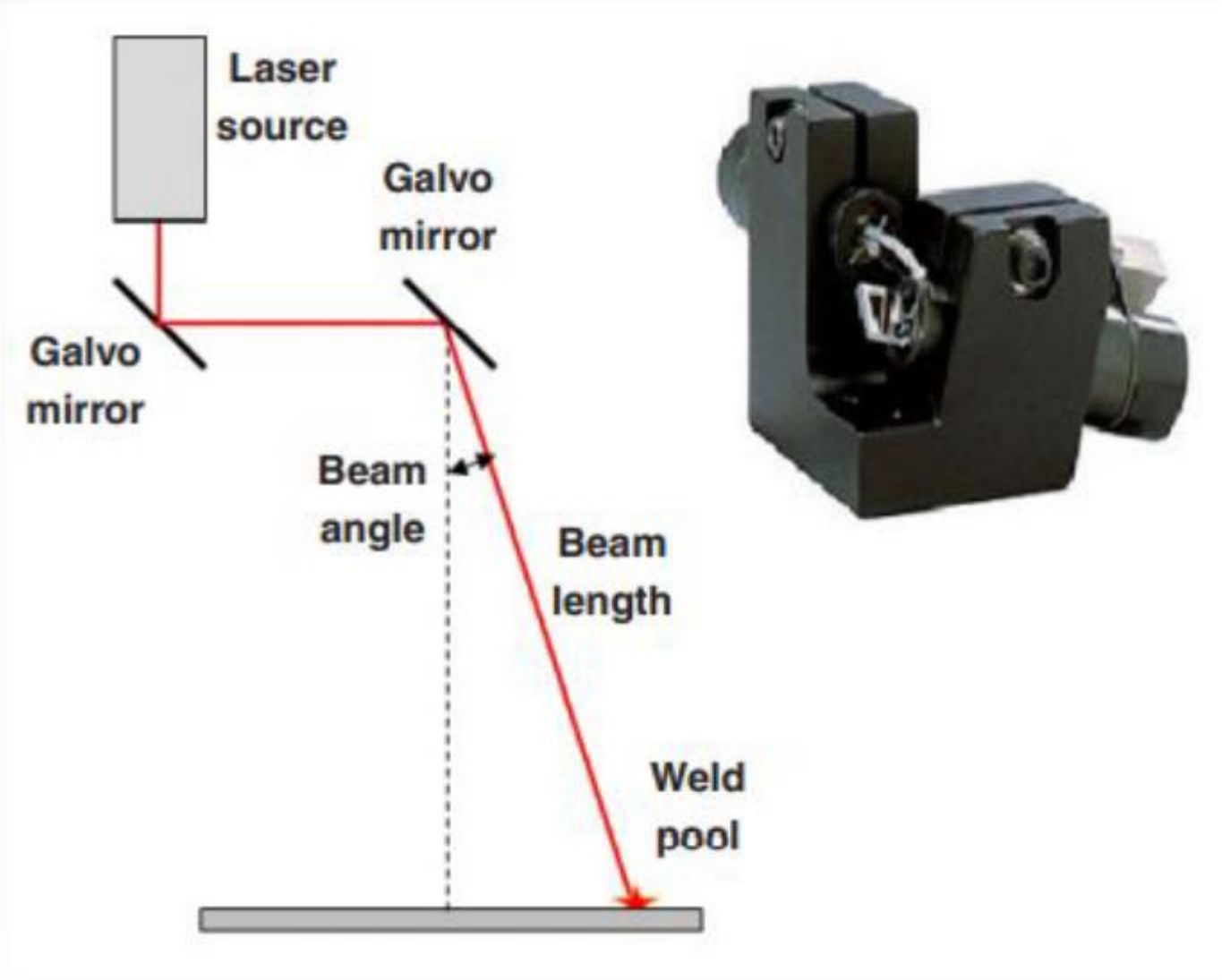

A direção do feixe é controlada por espelhos e lentes.
Na região central da plataforma, o feixe desce verticalmente.
Fora dessa região central, o ângulo incide na superfície com um certo ângulo.
Esse **ângulo do feixe** depende do tamanho da plataforma, do local onde estão os espelhos e as lentes.

Por exemplo, numa certa máquina, o maior ângulo de feixe, nas extremidades da plataforma, é de 7 graus.

Imagens de material disponível no site da Renishaw

Tipos de Laser (mais comum é o Nd:YAG)

Table 1 Representative lasers for additive manufacturing and those specifications[25]

Laser	CO_2 laser	Nd:YAG laser	Yb-fiber laser	Excimer laser
Application	SLA, SLM, SLS, LENS	SLM, SLS, LENS	SLM, SLS, LENS	SLA
Operation wavelength	9.4 & 10.6 μm	1.06 μm	1.07 μm	193, 248, and 308 nm (ArF, KrF, and XeCl respectively)
Efficiency	5 - 20 %	Lamp pump: 1-3 %, Diode pump: 10-20 %	10 - 30 %	1 - 4 %
Output power (CW)	Up to 20 kW	Up to 16 kW	Up to 10 kW	Average power 300 W
Pump source	Electrical discharge	Flashlamp or laser diode	Laser diode	Excimer recombination via electrical discharge
Operation mode	CW & Pulse	CW & Pulse	CW & Pulse	Pulse
Pulse duration	Hundreds ns-tens μs	Few ns – tens ms	Tens ns – tens ms	Tens ns
Beam quality factor (mm·mrad)	3 - 5	0.4 - 20	0.3 - 4	160 × 20 (Vertical × Horizontal)
Fiber delivery	Not possible	Possible	Possible	Specially designed fiber necessary
aintenance periods	2000 hrs	200 hrs (lamp life) 10,000 hrs (diode life)	Maintenance free (25,000 hrs)	10^{8-9} pulses (thyratron life)

Nd-YAG: Ytrium Aluminum Garnet : Granada de Al e Y dopada com Nd:$Y_3Al_5O_{12}$

Granada é o nome de um mineral do tipo $A_3B_2(SiO_4)_3$.

Laser pode ser contínuo, pulsado (e modulado)

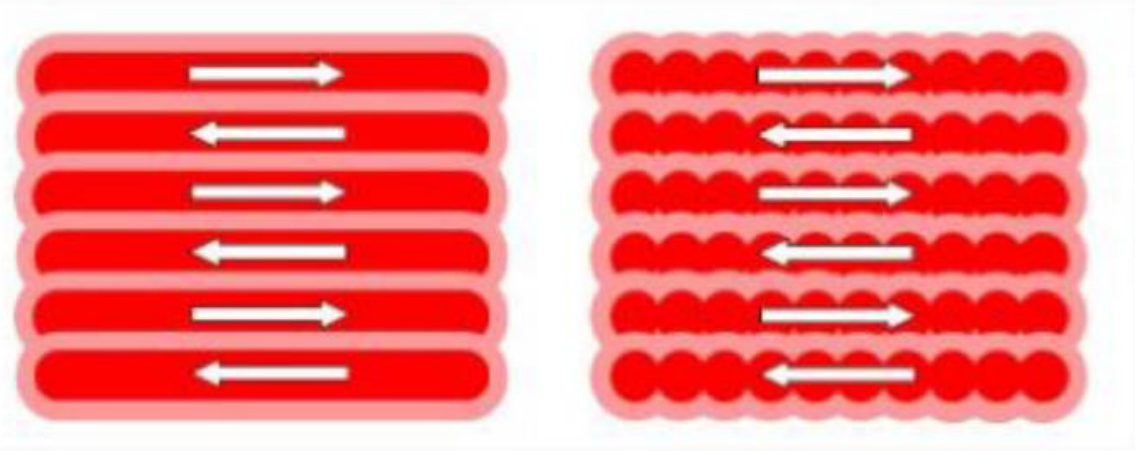

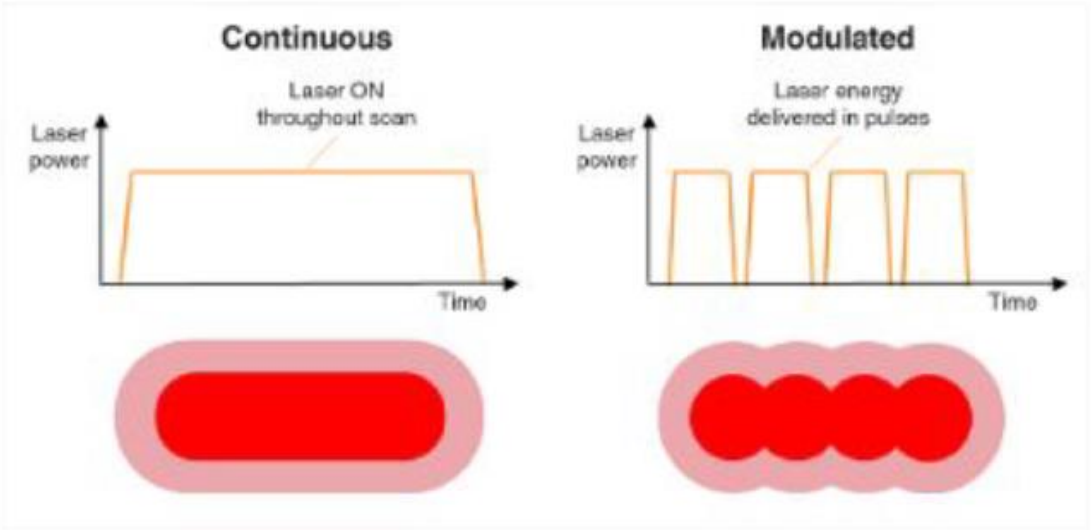

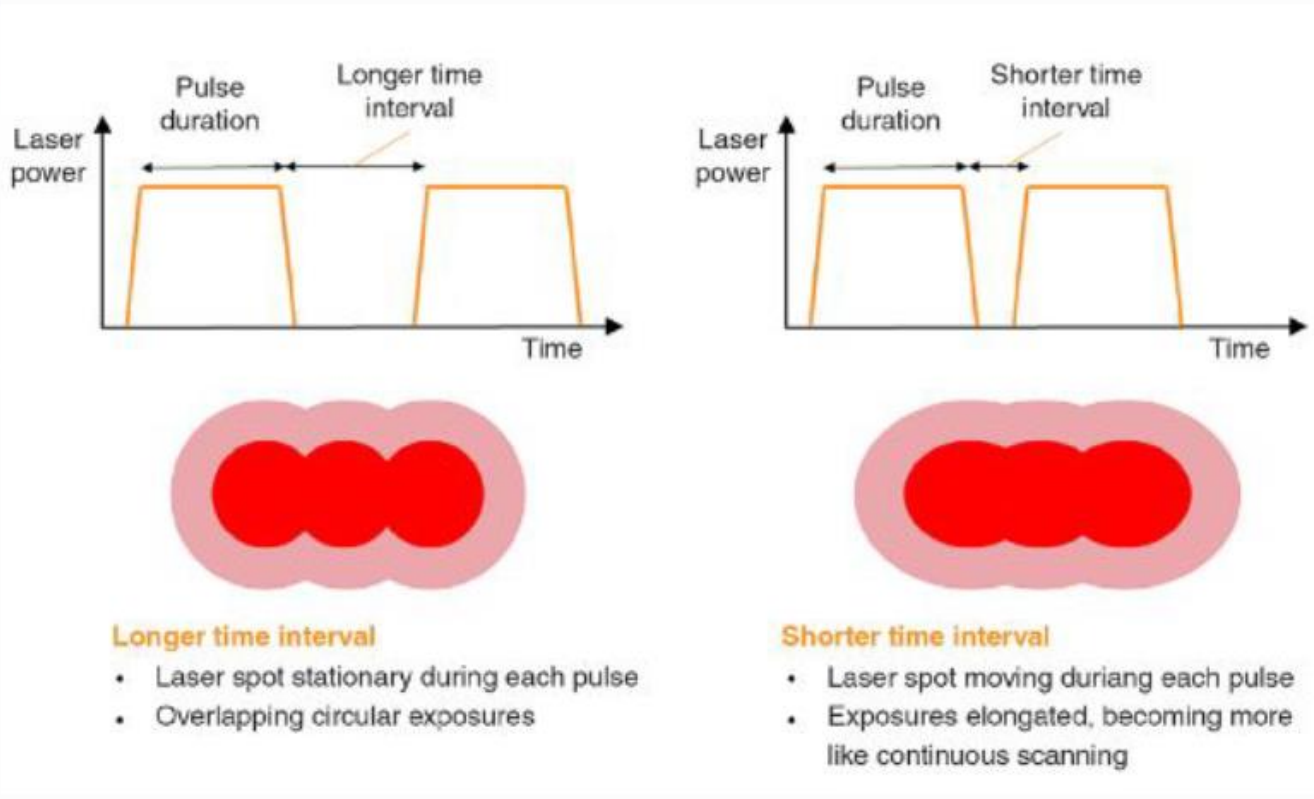

Imagens de material disponível no site da Renishaw

Contínuo x pulsado

- Maior parte dos fabricantes usam laser contínuo
- Renishaw é o mais famoso fabricante que usa pulsado.

Potenciais vantagens do laser pulsado

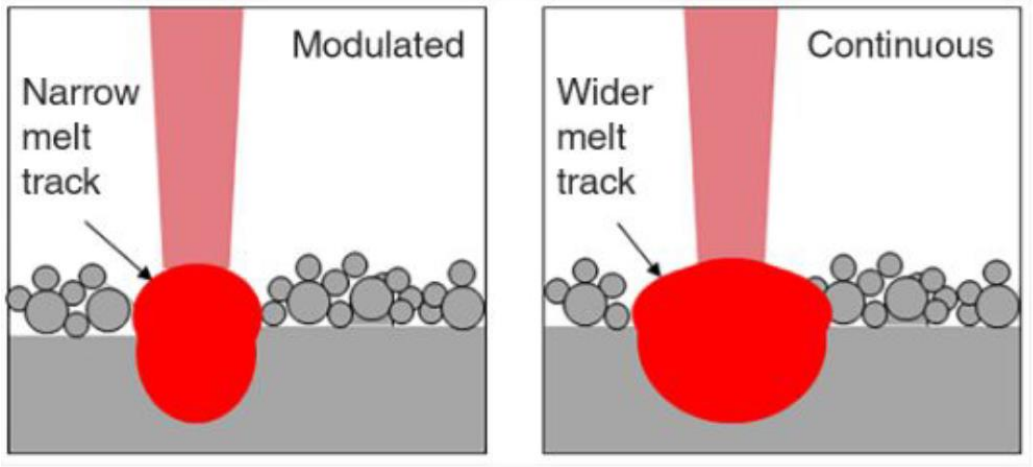

A exposição modulada produz uma trilha mais estreita para uma determinada profundidade de penetração.
Bom para detalhes.

Overhanging

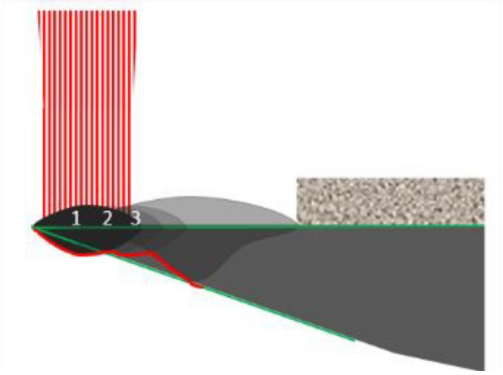

Exposições moduladas curtas são eficazes em limitar a penetração de energia

Imagens de material disponível no site da Renishaw

Absorbância

- Da energia da luz incidente, parte é refletiva, parte absorvida e parte transmitida.
- I=T+R+A
- Nos metais, opacos, T=0
- Então I=R+A=1
- Ou, se R=0,9, A=0,1.

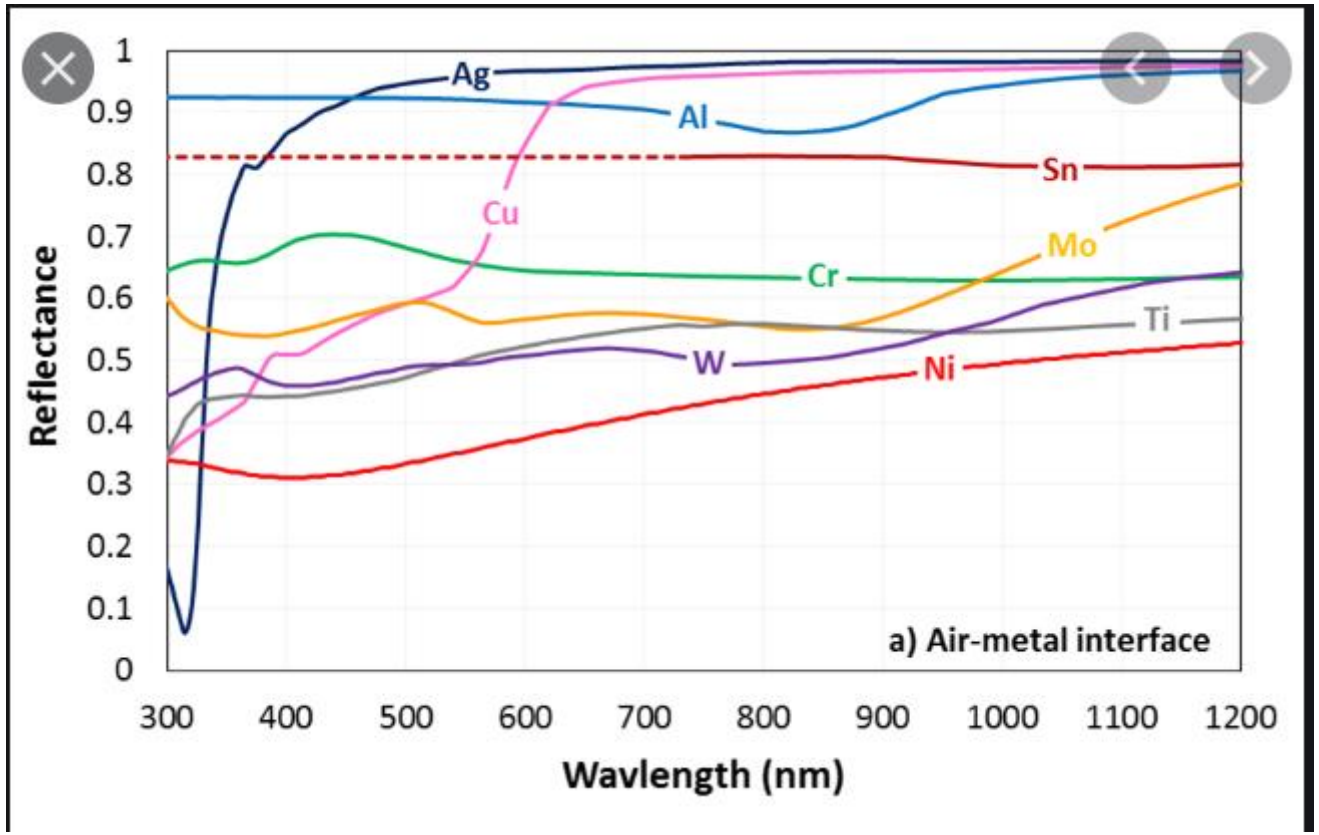

Refletância em superfície polida

O Centro de Laser e Aplicações do IPEN mede absorbância

- Resultados de medida de dois tipos de pó da liga Ti13Nb13Zr
- Pó esférico, atomizado a água:
  - Absorbância de 74%
- Pó irregular produzido por Hidrogenação-moagem-desidrogenação:
  - Absorbância de 80%

Feixe de Elétrons

- Usam lentes eletromagnéticas
- Diâmetro do feixe tipicamente de 200 µm
- Determinam potência usando Copos de Faraday
- Determina-se densidade de energia no feixe usando Copos de faraday modificados ou detetores “Pinhole”.

Arco elétrico

- power density distribution is affected by
  - arc length,
  - filler wire diameter,
  - arc current
  - Nature of the shielding gas In particular, the pulsed current
- commonly determined by an appropriate split anode technique. sources are used for the electric arc assisted wire-fed AM processes.
- The pulsating nature of current allows high peak pulse for a short duration that helps in superior control on filler wire deposition and heat input.
- Spot size of an electric arc varies in the range of a few millimeters.
- plasma arc being more concentrated than a gas metal arc.

Escolha da fonte de potência

- Depende da taxa de deposição
- Da resolução dimensional
-

2.4. Interação entre as fontes de calor e as matérias primas

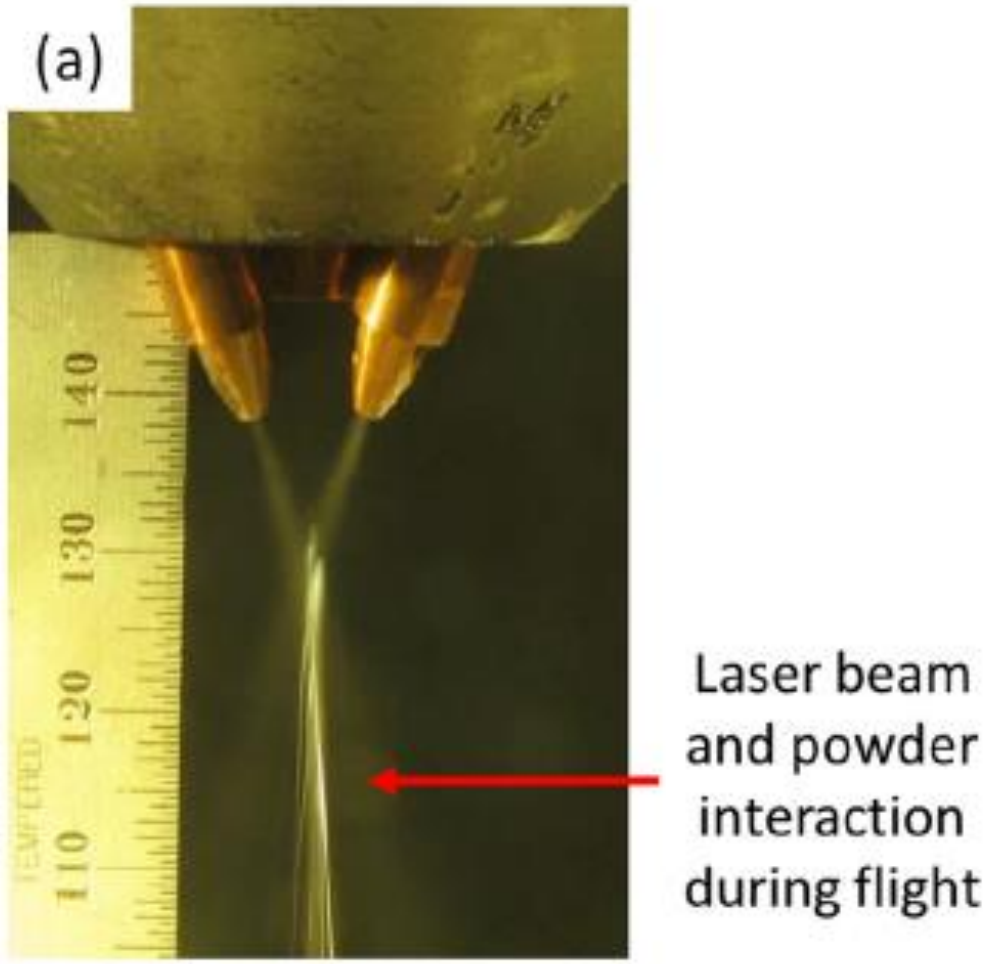

A evolução do Campo de Temperatura, durante um processo DED, depende da absorção de calor pela matéria prima

In DED processes, a fraction of the total heat is spent to heat the powder particles as they emerge from the nozzle and travel through the beam as shown in Fig. 4(a).
The heat absorbed by the particles in-flight depends on their density and thermo-physical properties, shape and size distribution, free flight duration through the beam, and gas velocity [79].
The powder particles are usually heated to a higher temperature although they do not reach their melting temperature [79].
The remaining beam energy impinges on the deposit surface resulting in a small molten pool. The extent of energy absorbed by the deposit surface also depends on beam characteristics, deposit geometry and the shielding gas [79].

[79] Manvatkar V, De A, DebRoy T. Heat transfer and material flow during laser assisted multi-layer additive manufacturing. J Appl Phys 2014;116(12): Article No. 124905

Densidade de Energia absorvida no DED

- The heat source in DED process can be represented by the following volumetric heat source with a modified Gaussian distribution [79].

$$P_d = \frac{fP}{\pi r_b^2 t_l}\left[\eta_P + (1-\eta_P)\eta_l\right]\exp\left(-f\frac{r^2}{r_b^2}\right)$$

- where η_p is the fraction of energy absorbed by the powder during flight,
- η_l refers to the absorption coefficient of the deposit,
- and t_l is the layer thickness.

- A higher value of f indicates higher power density at the heat source axis and vice versa
- a larger layer thickness indicates lower power density at all radial locations and vice versa.
- The value of the absorption is high when the powder is solid, however after a short time (a few milliseconds) the liquid surface absorbs energy by Fresnel absorption .
- So, the value of η_l is high initially when the liquid layer is forming but reduces once the surface melts.
- For a laser assisted DED process with Argon as shielding gas, the absorption coefficients for a laser beam of 1064 μm wavelength remain between 0.3 and 0.7 depending on whether the deposit is in liquid or solid state

Absorção de energia no processo PBF

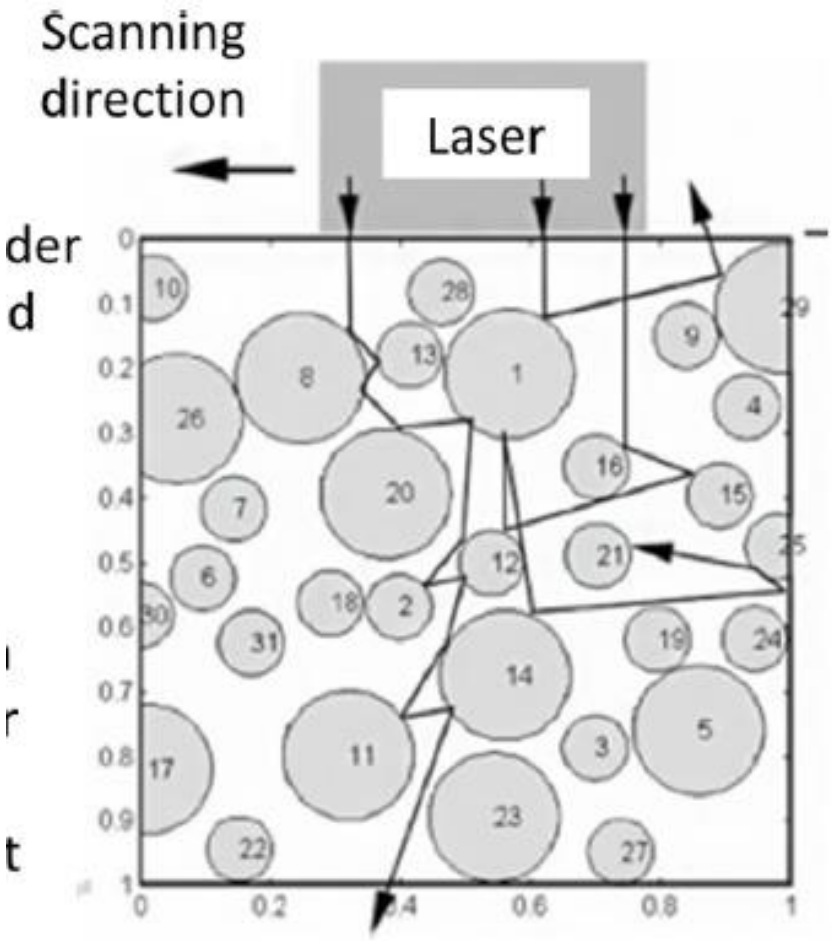

- In case of the PBF processes, the entire amount of heat source energy is incident on the powder bed.
- When a laser beam impinges on a particle, part of the energy is absorbed by the particle and the rest is reflected that continues until the beam emerges outside of the powder bed or its intensity becomes negligible.
- As the beam undergoes multiple reflections within the powder layers, the coefficient of beam absorption by the powder bed is higher than the Fresnel absorption coefficient of the liquid surface.
- The heat absorbed by the particles in powder-bed depends on the particle size, packing density of the powder bed and material properties.

Absorbância na cavidade líquida no PBF-L

- Nas densidades de energia normalmente usadas no PBF-L, a temperatura do líquido aumenta tanto que ocorre significativa evaporação.
- O gás evaporado cria uma pressão que forma uma cavidade na poça líquida , aumentando as reflexões do laser dentro da cavidade, o que aumenta a absorbância e aprofunda a cavidade: é a formação do “keyhole”, que discutiremos mais a frente.

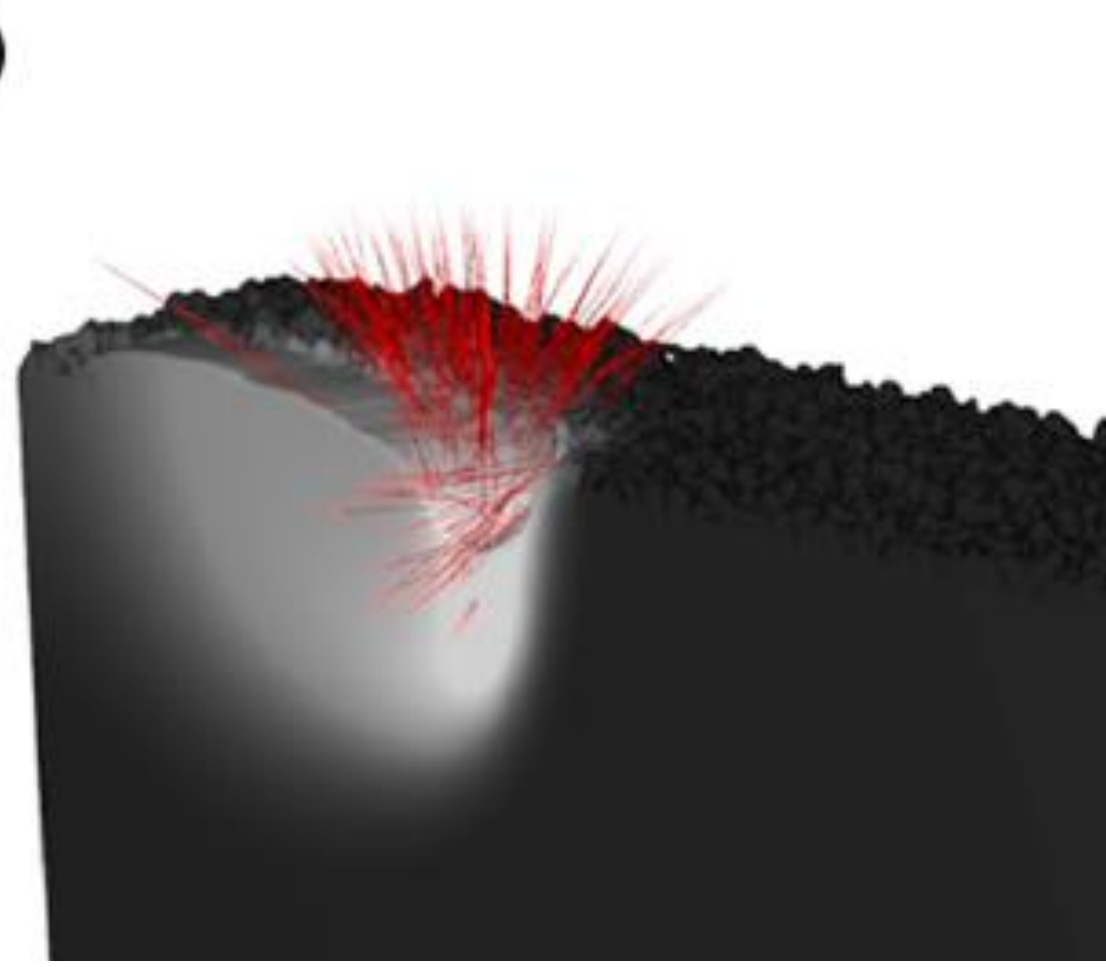

Keyhole-induced porosities in Laser-based Powder Bed Fusion (L-PBF) o
Ti6Al4V: High-fidelity modelling and experimental validation

Mohamad Bayat[a,*], Aditi Thanki[b], Sankhya Mohanty[a], Ann Witvrouw[b], Shoufeng Yang[b],

Definições de densidade de energia

- Dentre as variáveis de processo na M.A., além das variáveis imediatas, como potência do laser (P), diâmetro do feixe (d), velocidade de varredura (v), distância entre passes (hs) , espessura de camada (t), densidade aparente da camada (dap), é possível definir variáveis que sintetizam parâmetros:
- Densidade linear de energia El = P/v (J/m)
- Densidade volumétrica de energia Ev = P / (v.t.hs) (J/m3)
- Densidade mássica de energia Em = Ev / dap (J/kg)
- Entalpia normalizada $\frac{\Delta H}{h_s} = \frac{AP}{h_s\sqrt{\pi d v \sigma^3}}$ (adimensional)
- Onde A é a absorbância do laser naquela liga, d é a difusividade térmica, sigma é o raio do feixe e hs é a entalpia na Tfusão, em J/m3.

A entalpia normalizada não tem sido muito usada

$$\frac{\Delta H}{h_s} = \frac{AP}{h_s\sqrt{\pi d v \sigma^3}}$$

- A é a absorbância do laser naquela liga, d é a difusividade térmica, sigma é o raio do feixe e hs é a entalpia na $T_{fusão}$, em J/m3.
- Curioso não entrar a espessura da camada

Porosidade causada por poça profunda de aquecimento localizado (keyhole) , no PBF-L

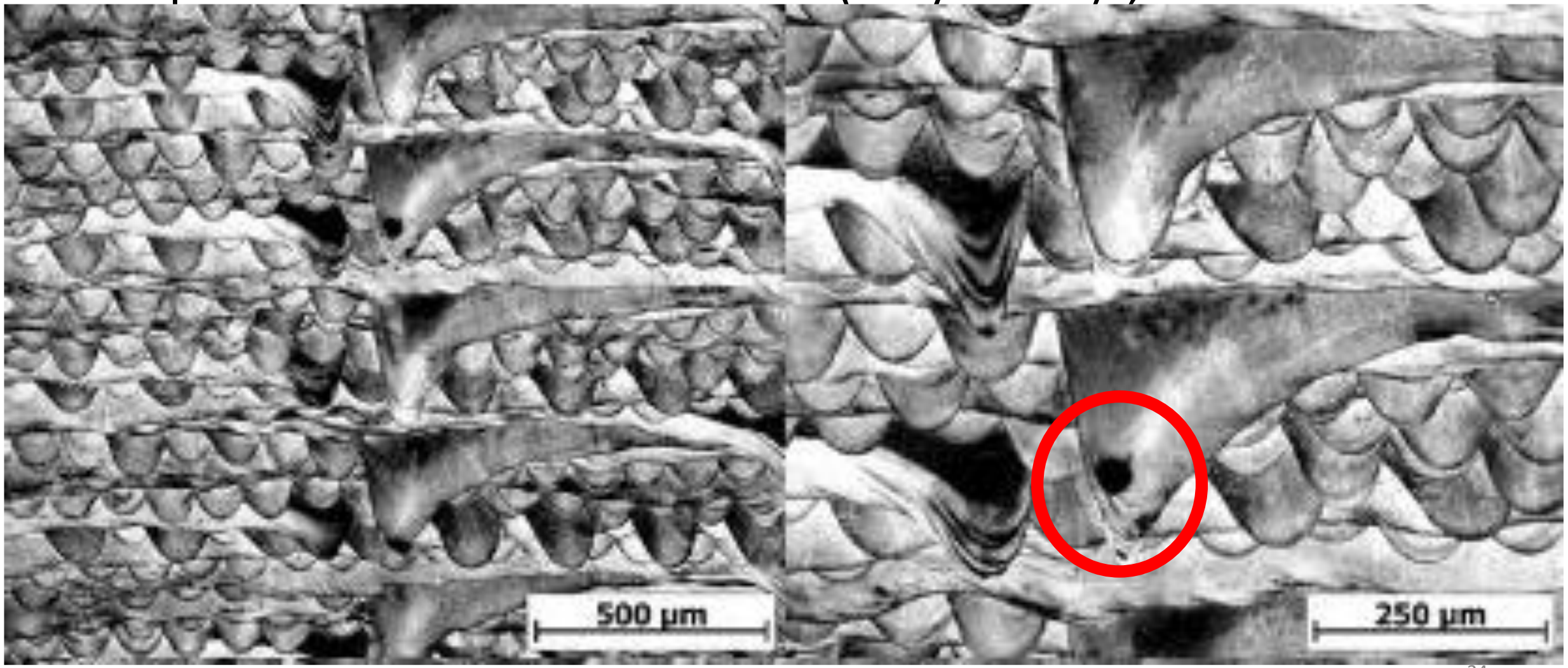

Poça profunda pode ocorrer quando o laser inverte seu sentido para percorrer uma trilha paralela.

Existem ajustes de parâmetros dos espelhos que permitem evitar o superaquecimento local.

Por exemplo, na borda de cada “ilha”, o laser se move lateralmente e inverte seu sentido. Naquela região amarela, o laser fica mais tempo do que nas outras regiões, mesmo que a velocidade fosse constante.

Além disso, parâmetros do acoplamento eletrônico-mecânico dos espelhos podem aumentar o tempo de passagem do laser naquela região.

Observar o caminho e o tamanho da poça de fusão:

Frenagem e reversão com potência constante

Frenagem e reversão com mitigação de potência.

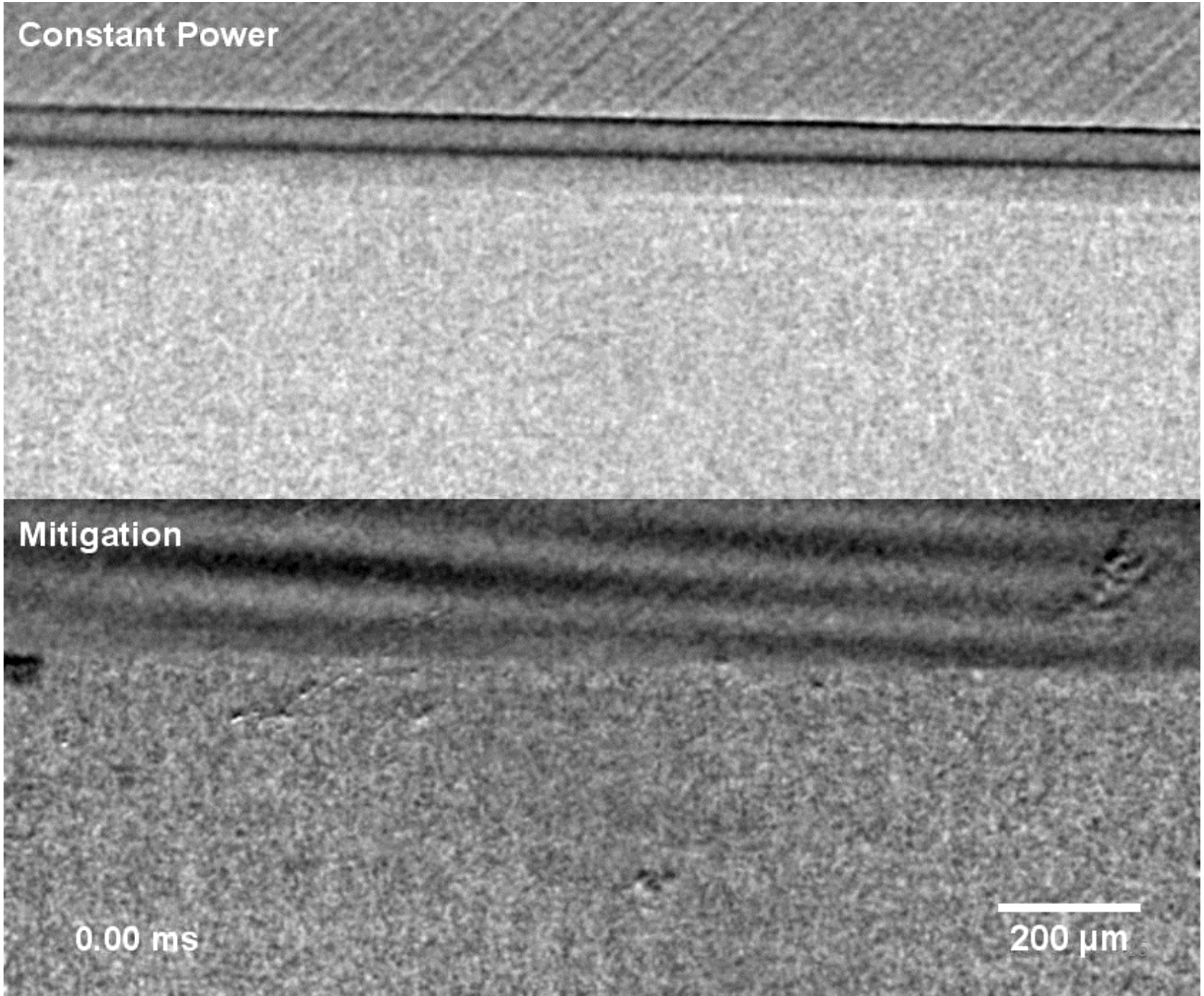

Spatter

- At high power densities the powder particles or the molten droplets may be ejected from the molten pool resulting in spatter formation.
- The molten pool experiences significant recoil pressure due to local vaporization of alloying elements and the molten droplets may be ejected when the recoil pressure is higher than the surface tension force at the periphery of the liquid pool.
- During PBF-EB powder particles may also be ejected due to the high repulsive electrostatic force.

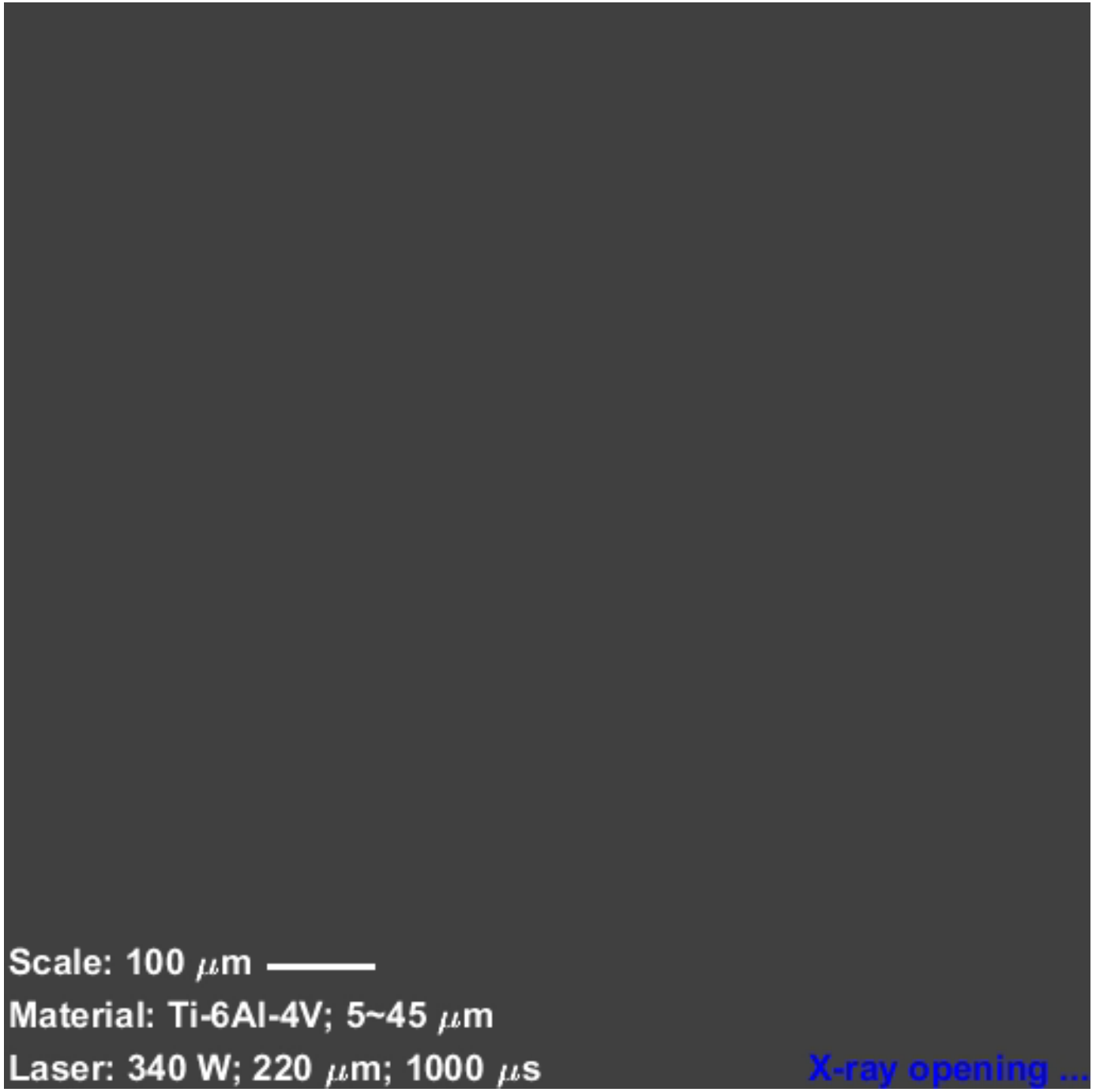

Formação do Spatter em PBF-L

filme feito por raios X, numa trilha de 220um,
com formação de poça profunda (keyhole).

Spatter é a projeção de gotas de metal líquido.

2.5. Princípios de transferência de calor e massa e de fluxo de líquido.

- No caso de PBF, e mesmo de DED, a microestrutura do material e suas propriedades são formadas por solidificação rápida, seguida de sucessivos reaquecimentos e resfriamentos, conforme a a fonte de calor de movimenta.
- Devido à natureza aditiva do processo, medidas experimentais de temperatura só são possíveis em superfícies de fácil acesso, mas não em locais no interior do material.

modelamento

- Para poder prever as distorções, tensões residuais e microestrutura resultante desses complexos ciclos térmicos, é necessário modelar o movimento dos campos térmicos tridimensionais que ocorrem nesses processos. Esse tipo de estudo está avançando rápido.

Nat Commun. 2019; 10: 1987.
Published online 2019 Apr 30. doi: 10.1038/s41467-019-10009-2

Dynamics of pore formation during laser powder bed fusion additive manufacturing

Aiden A. Martin,[1] Nicholas P. Calta,[1] Saad A. Khairallah,[1] Jenny Wang,[1] Phillip J. Depond,[1] Anthony Y. Fong,[2] Vivek Thampy,[2] Gabe M. Guss,[1] Andrew M. Kiss,[2] Kevin H. Stone,[2] Christopher J. Tassone,[2] Johanna Nelson Weker,[2] Michael F. Toney,[2] Tony van Buuren, [1] and Manyalibo J. Matthews

[1]Lawrence Livermore National Laboratory, Livermore, CA 94550 USA
[2]Stanford Synchrotron Radiation Lightsource, SLAC National Accelerator Laboratory, Menlo Park, CA 94025 USA

Formação de poros no PBF-L

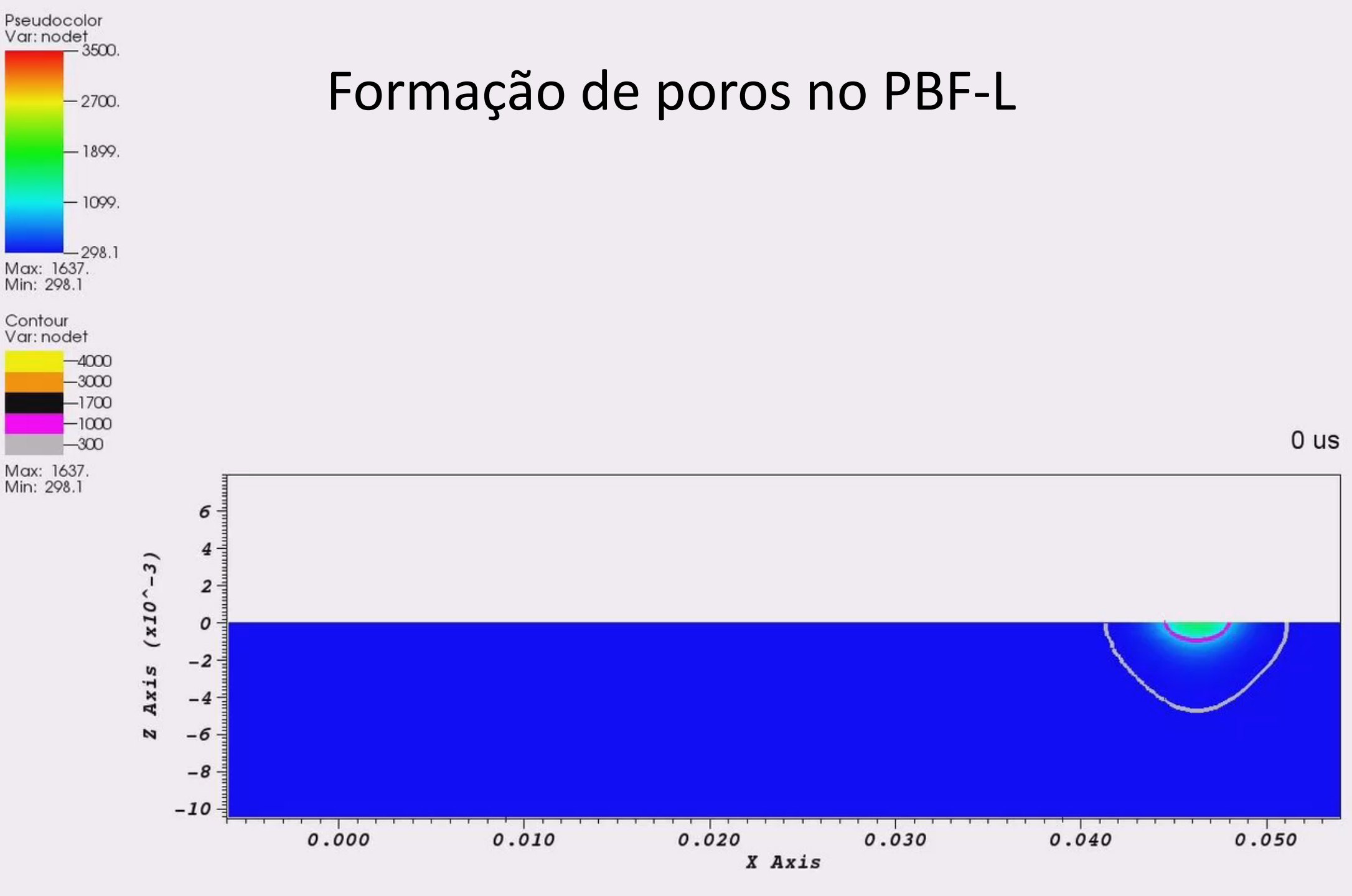

- PBF e DED se parecem mais com soldagem do que com fundição, mas cada processo tem diferenças importantes:
- Na soldagem, metal sólido cerca a zona de fusão, o que não ocorre na M.A.
- A fonte de calor interage de forma muito diferente com uma cama de pós, ou uma corrente descendente de pós ou um fio,
- É necessário levar em conta a construção progressiva das camadas, variações na geometria das camadas, os múltiplos ciclos térmicos,

Equações da conservação de massa, momento e energia

$$\frac{\partial(\rho u_i)}{\partial x_i} = 0$$

$$\frac{\partial(\rho u_j)}{\partial t} + \frac{\partial(\rho u_j u_i)}{\partial x_i} = \frac{\partial}{\partial x_i}\left(\mu \frac{\partial u_j}{\partial x_i}\right) + S_j$$

$$\rho \frac{\partial h}{\partial t} + \frac{\partial(\rho u_i h)}{\partial x_i} = \frac{\partial}{\partial x_i}\left(\frac{k}{C_p}\frac{\partial h}{\partial x_i}\right) - \rho \frac{\partial \Delta H}{\partial t} - \rho \frac{\partial(u_i \Delta H)}{\partial x_i}$$

where ρ is the density, u_i and u_j are the velocity components along the i and j directions, respectively, and x_i is the distance along the i direction, t is the time, μ is the dynamic viscosity, S_j is a source term for the momentum equation, h is the sensible heat, C_p is the specific heat, k is the thermal conductivity, and ΔH is the latent heat content. The source term S_j considers buoyancy and electromagnetic forces (the latter is applicable when an arc or electron beam is used). Buoyancy force plays a minor role in molten pool convection and does not affect heat transfer and fluid flow in AM. For the electric arc assisted AM, electromagnetic force is also responsible for the molten metal flow and is considered for the calculations of heat transfer and fluid flow in the melt pool.

2.5.1 Condições de contorno

- O fluxo convectivo do metal líquido dentro da poça é movido pelo efeito Marangoni: o gradiente térmico no topo da poça líquida cria um gradiente de tensão superficial que origina a tensão de Marangoni, dirige o fluxo de líquido dentro da poça.
- A tensão de cisalhamento de Marangoni, na superfície da poça líquida, é dada por

$$\tau_M = \frac{d\gamma}{dT}\frac{dT}{dr} = -\mu\frac{du_i}{dx_k}$$

- where T is the temperature, γ is the surface tension, τ_M is the Marangoni stress, r is the radial distance from the axis of the heat source,
- μ_i is the velocity component in the i direction and x_k is the distance along k direction which is the vertical direction

Efeito Marangoni

Entry #V0020

Marangoni Bursting: Evaporation-Induced Emulsification of a Two-Component Droplet

Guillaume Durey[1], Hoon Kwon[1], Julien Mazet[2], Quentin Magdelaine[1], Mathias Kasiulis[1], Ludovic Keiser[3], Hadrien Bense[3], Pierre Colinet[4], José Bico[3], Étienne Reyssat[3]

1 The Lutetium Project, ESPCI Paris, PSL Research University, youtube.com/thelutetiumproject
2 Conservatoire National Supérieur de Musique et de Danse de Paris, PSL Research University
3 Laboratoire PMMH, CNRS, ESPCI Paris, PSL Research University, Sorbonne Université, Université Paris Diderot
4 Transferts, Interfaces et Procédés, Université Libre de Bruxelles

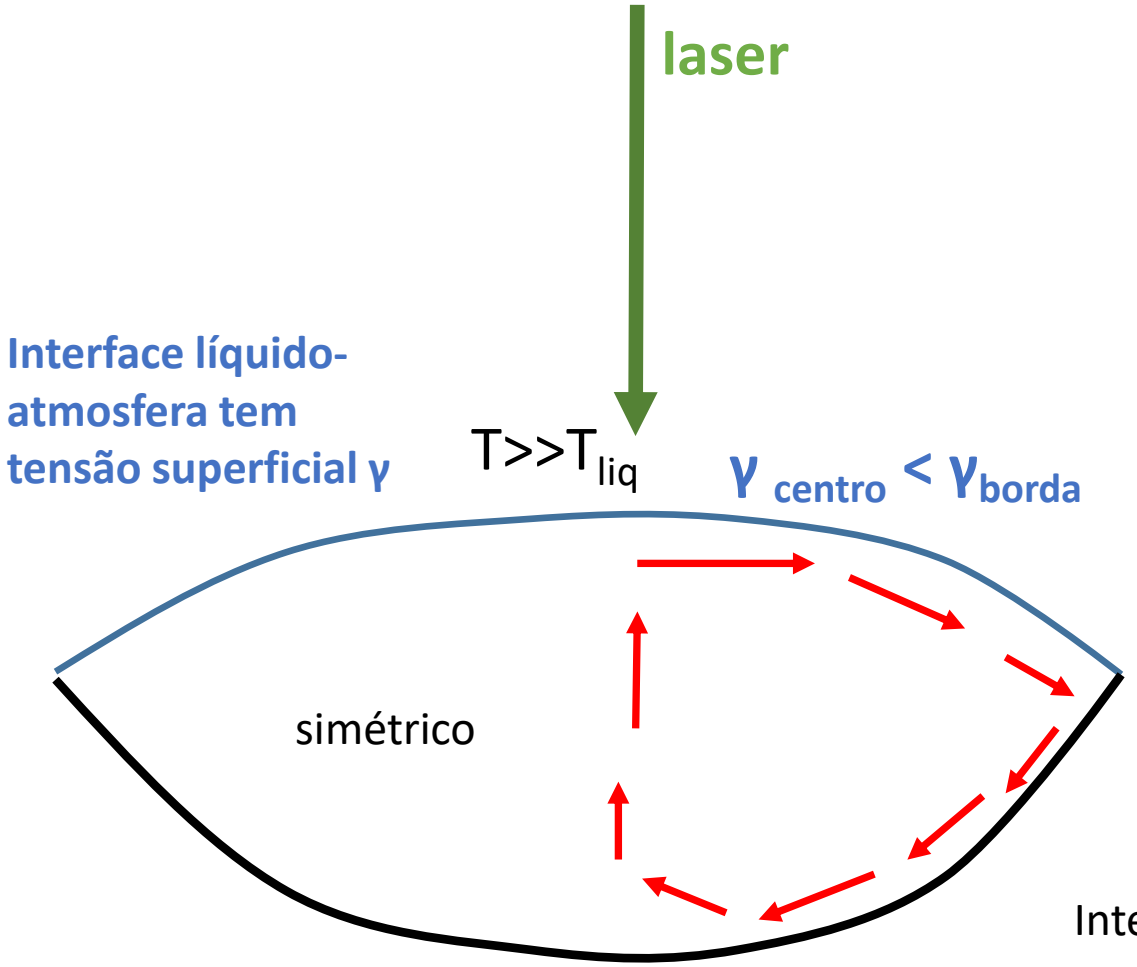

Em metais puros, ou ligas sem tensoativos,
dγ/dT é negativo: o aumento da temperatura diminui a tensão superficial.

Líquido com baixa tensão superficial se espalha, indo do centro para a borda da poça: leva o calor do centro para a borda.

Resultado: poça rasa

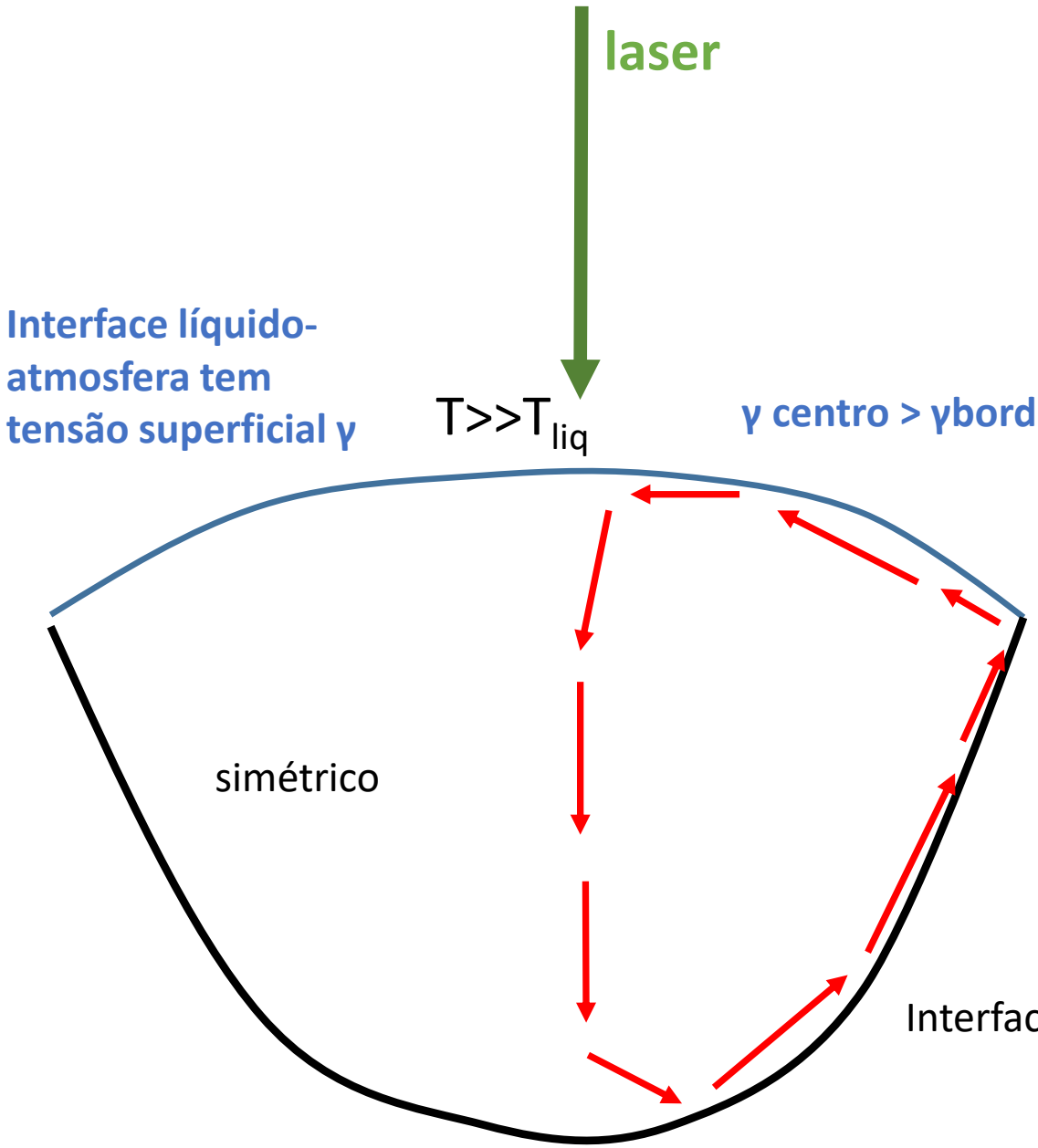

Em ligas com tensoativos, dγ/dT é positivo: o aumento da temperatura aumenta a tensão superficial.

Líquido com baixa tensão superficial se espalha, indo da borda para o centro da poça, e dali para baixo! leva o calor para baixo.

Resultado: poça funda

Efeito de tensoativos

- The surface tension of metals and alloys depends on temperature and composition.
- The concentrations of surface active elements in alloys, i.e., the elements that have a tendency to migrate to the surface of the liquid, affect the surface tension of alloys significantly.
- Examples of these elements include common alloying elements such as oxygen, sulfur, selenium, tellurium and nitrogen in steels

Efeito de tensoativos

- For pure metals and alloys containing no surface active elements, the temperature coefficient of surface tension, dγ/dT is negative. As a result, the hot packets of liquid metal carry heat from the middle of the liquid pool to its periphery, and the molten pool becomes wide and shallow.
- However, when an alloy contains a surface active element, the value of the temperature coefficient of surface tension may become positive except at very high temperatures close to the boiling point of the alloy.

Efeito do teor de S e da Temp. na tensão superficial de ferro

- In those cases, the liquid metal flows in a direction opposite to that in the absence of sulfur. Specifically, the convective heat flow carries heat downward in the middle of the liquid pool making the liquid pool deep and narrow

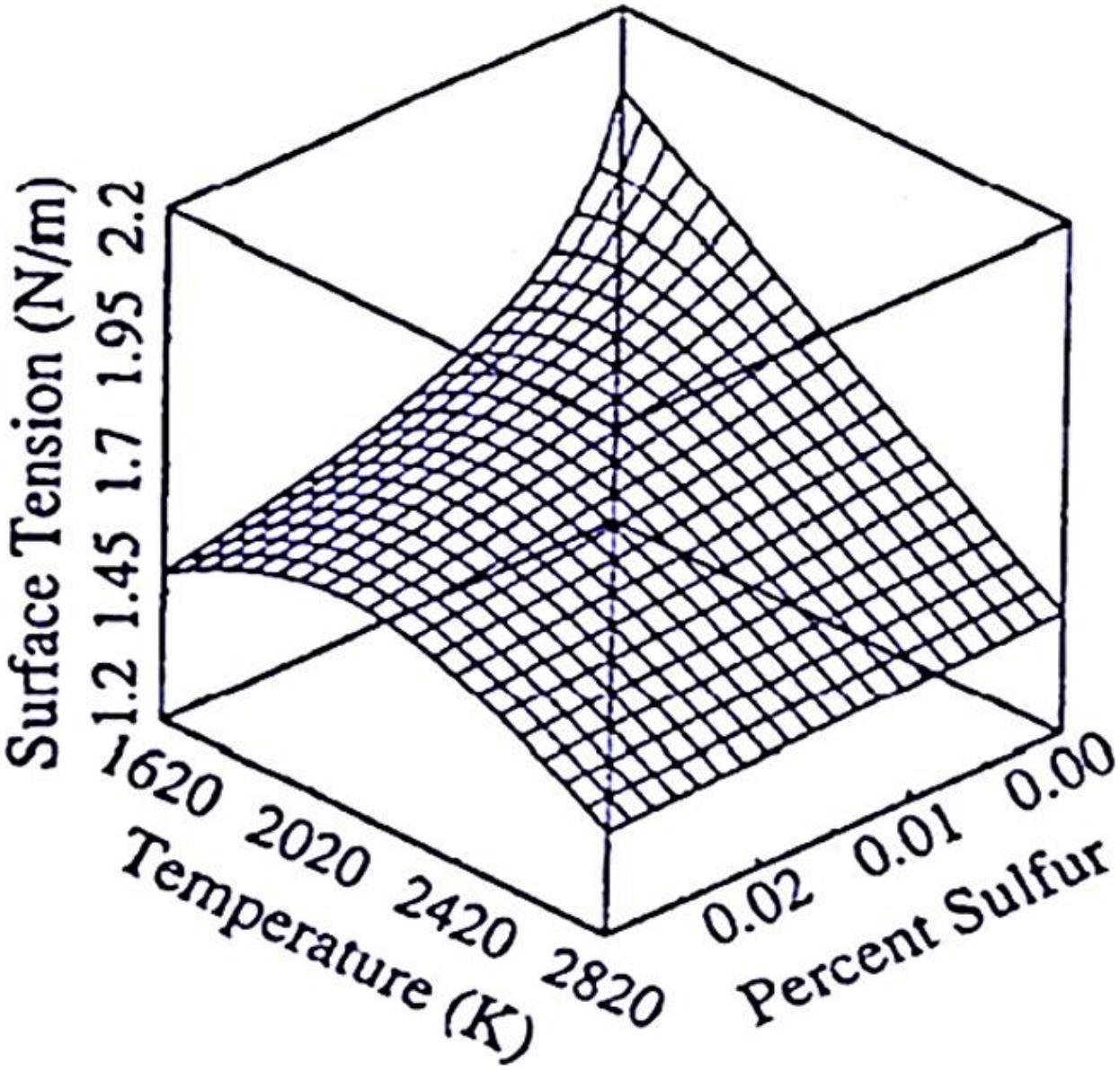

- The velocity component perpendicular to the free surface and all velocity components at the solid-liquid interface are taken as zero.
- The boundary condition for the heat exchange between the top surface of the build and the surroundings involves consideration of both convective and radiative heat transfer:

$$-k\frac{\partial T}{\partial Z} = \sigma_{SB}\varepsilon(T^4 - T_a^4) + h_c(T - T_a)$$

where σ_{SB} is the Stefan-Boltzmann constant (5.67×10^{-8} W m^{-2} K^{-4}), ε is the emissivity, T_a is the ambient temperature and h_c is the convective heat transfer coefficient. Significant variations in the heat transfer rates can occur depending on the

Princípios do modelamento: as células.

- In all numerical calculations of temperature and velocity fields, the computational domain is subdivided into many small control volumes or cells and appropriate temperature dependent thermo-physical properties are assigned to each of these cells.
- Properties of these cells change with time as temperature changes or new materials are added to the build.
- Additions of mass may be simulated either by changing properties of existing cells or by adding new cells with appropriate thermo-physical properties.

Table 4
Thermo-physical properties of commonly used alloys in AM [102,103]

Alloy	Liquidus temperature (K)	Solidus temperature (K)	Density (kg/m^3)	Viscosity (kg/m s)	$d\gamma/dT$ (N/m K)	Thermal conductivity[a] (W/m K)	Specific heat[a] (J/kg K)
SS316	1733	1693	7800	7×10^{-3}	-0.40×10^{-3}	$A = 11.82$ $B = 0.0106$	$A = 330.9$ $B = 0.563$ $C = -4.015 \times 10^{-4}$ $D = 9.465 \times 10^{-8}$
Ti-6Al-4V	1928	1878	4000	4×10^{-3}	-0.26×10^{-3}	$A = 1.57$ $B = 1.6 \times 10^{-2}$ $C = -10^{-6}$	$A = 492.4$ $B = 0.025$ $C = -4.18 \times 10^{-6}$
IN 718	1609	1533	8100	5×10^{-3}	-0.37×10^{-3}	$A = 0.56$ $B = 2.9 \times 10^{-2}$ $C = -7 \times 10^{-6}$	$A = 360.4$ $B = 0.026$ $C = -4 \times 10^{-6}$
H13 steel	1725	1585	7900	7×10^{-3}	-0.43×10^{-3}	$A = 18.29$ $B = 7.5 \times 10^{-3}$	$A = 341.9$ $B = 0.601$ $C = -4.04 \times 10^{-6}$
AA6061	925	855	2700	–	–	$A = 2.52$ $B = 0.4 \times 10^{-2}$ $C = -7.36 \times 10^{-6}$	$A = 929.0$ $B = -0.627$ $C = -1.48 \times 10^{-3}$

[a] Properties are expressed in terms of a polynomial with the form $A + BT + CT^2 + DT^3$ where T is temperature in K.

Modelos

- Different analytical and numerical approaches have been used to understand the heat transfer and the flow of molten metal.
  - analytical approach [104–106],
  - heat conduction models [107–116],
  - heat transfer and fluid flow models [79,92,93,117–119],
  - level set method [120–123],
  - volume of fluid method [124,125],
  - Lattice Boltzman and
  - Arbitrary Lagrangian Eulerian methods [59,126–130].
- Many of the previous studies have considered temperature dependent thermal conductivity and specific heat for the work-piece [27,131,132].

Table 5
Comparison among the current approaches for heat and fluid flow calculations in AM.

Approaches	Features
Analytical approach	• Analytically solves Rosenthal's heat conduction equation. • Outputs are temperature fields, build dimensions and cooling rates. • Computationally less expensive, simplified and easy to use. • Ignores the dominant mechanism of heat transfer and known to produce large errors.
Heat conduction models using finite element method (FEM)	• Solves steady state or transient energy conservation equation with convective and radiative boundary conditions. • Outputs are 3D steady state or transient temperature distribution and build shape and size. • Many existing software packages, easy to implement, can handle intricate geometries. • Does not consider the effects of convective flow of liquid metal inside molten pool on the temperature field, therefore severely overestimates the peak temperature and cooling rate.
Heat transfer and fluid flow models using finite difference method (FDM)	• Solves 3D transient conservation equations of mass, momentum and energy. • Outputs are 3D transient temperature and velocity distributions, build shape and size, solidification parameters. • Considers the effects of molten pool flow inside pool and therefore provides accurate temperature distribution. • Often assumes flat top geometry of the deposit to make the calculations tractable.

Table 5
Comparison among the current approaches for heat and fluid flow calculations in AM.

Approaches	Features
Level set method (LSM)	• Tracks the free surface of the molten pool. • Outputs are 3D temperature and velocity distribution of the deposit with free curved surface. • The calculated deposit shape and size agree well with experiments. • Computationally intensive and tends to suffer from non-conservation of mass.
Volume of fluid (VOF) using finite difference method (FDM)	• Tracks the free surface of the molten pool. • Outputs are 3D temperature and velocity distribution of the deposit with free curved surface. • Computationally intensive. • Mass conservation maintained but at less sharp interface than LSM.
Lattice Boltzman method (LBM) and arbitrary Lagrangian–Eulerian (ALE)	• 2D and 3D numerical methods involving cellular automaton modeling of discrete particle kinetics by discrete space, time, and particle velocities. • It involves free surface boundary conditions treating thermodynamics, surface tension, phase transitions, and wetting. • Outputs are molten pool geometry and build shape and size. • Can predict the build geometry accurately. Also, the balling phenomenon and surface roughness can be simulated. • Computationally intensive however, suitable for massive parallel computing.

Os desafios:

- In AM processing, heating, melting, solidification, and cooling can occur very rapidly.
- The melt pool shape changes drastically due to coalescence and the movement induced by surface tension.
- Therefore, the dimensions of the molten pool and hence the consolidated build depend not only on the amount of heat supplied by the heat source but also controlled by the heat transfer and flow of molten metal within the liquid pool.
- Several attempts are also made to quantitatively explain how the heat transfer and fluid flow govern the molten pool shape, size and final microstructures and properties of the component using non-dimensional numbers.

Contents lists available at ScienceDirect

Acta Materialia

journal homepage: www.elsevier.com/locate/actamat

Full length article

Laser powder-bed fusion additive manufacturing: Physics of complex melt flow and formation mechanisms of pores, spatter, and denudation zones

Saad A. Khairallah*, Andrew T. Anderson, Alexander Rubenchik, Wayne E. King

Lawrence Livermore National Laboratory, 7000 East Ave. Livermore, CA 94550, USA

This study demonstrates the significant effect of the recoil pressure and Marangoni convection in laser powder bed fusion (L-PBF) of 316L stainless steel. A three-dimensional high fidelity powder-scale model reveals how the strong dynamical melt flow generates pore defects, material spattering (sparking), and denudation zones. The melt track is divided into three sections: a topological depression, a transition and a tail region, each being the location of specific physical effects. The inclusion of laser ray-tracing energy deposition in the powder-scale model improves over traditional volumetric energy deposition. It enables partial particle melting, which impacts pore defects in the denudation zone. Different pore formation mechanisms are observed at the edge of a scan track, at the melt pool bottom (during collapse of the pool depression), and at the end of the melt track (during laser power ramp down). Remedies to these undesirable pores are discussed. The results are validated against the experiments and the sensitivity to laser absorptivity is discussed.

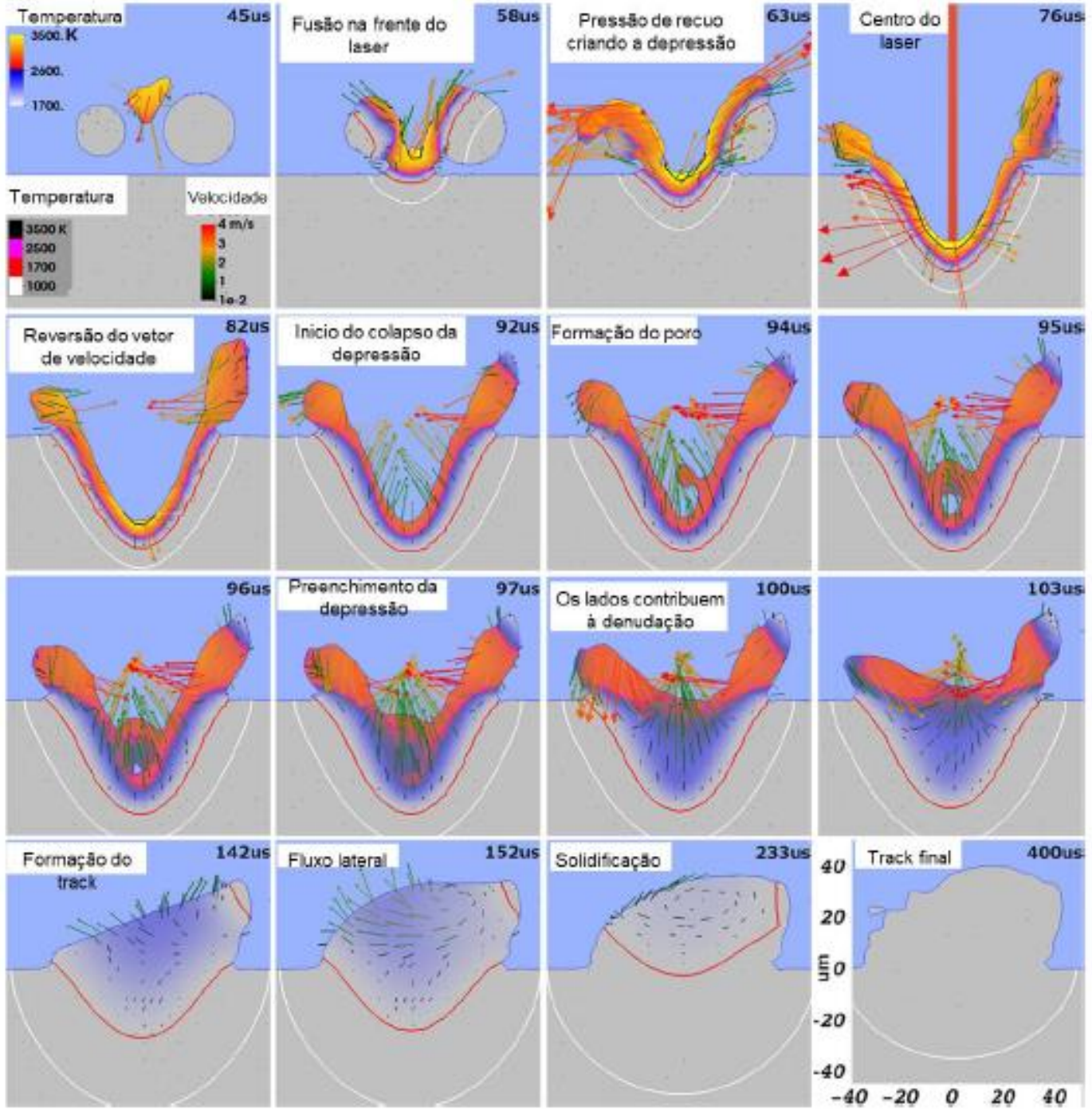

2.6. taxas de resfriamento, distribuição de temperatura e de velocidade.

- Para entender o processo é necessário conhecer, por exemplo, a taxa de resfriamento e a velocidade da interface sólido líquido. Portanto, é necessário conhecer os campos de temperatura.
- As temperaturas na poça de fusão podem chegar até a ebulição, ou seja, centenas de graus acima da Tf.
- É possível usar termovisão de infravermelho para estimar as temperaturas na superfície da poça.
- Para validar um modelamento, é necessário medir temperaturas pelo menos a certa distância da poça. Pode-se usar termopares para isso.

Exemplo de modelamento

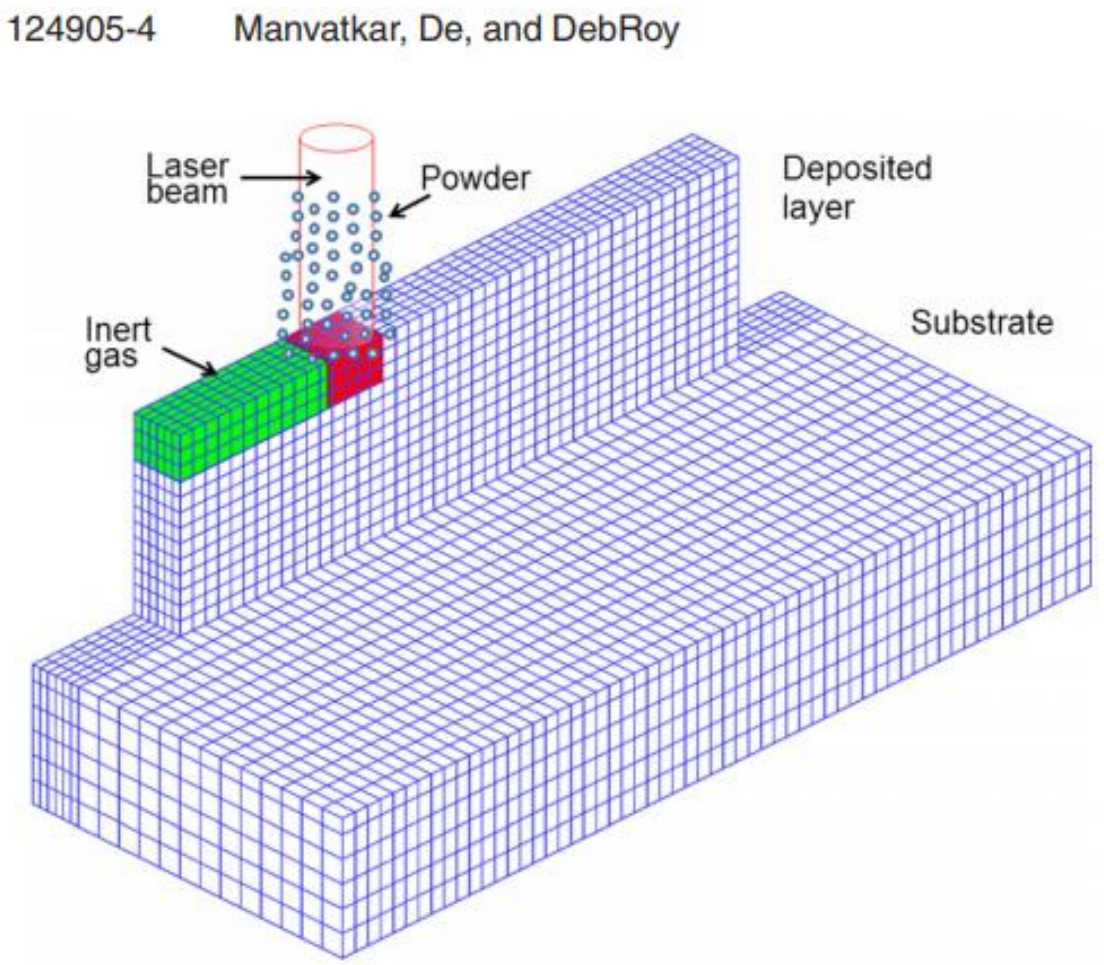

- Referencia 79: DED-L
- Typically a total of 26 000 iterations were necessary per layer and a total of 13.5 billion linear equations were solved cumulatively for all time steps for a three layer structure.

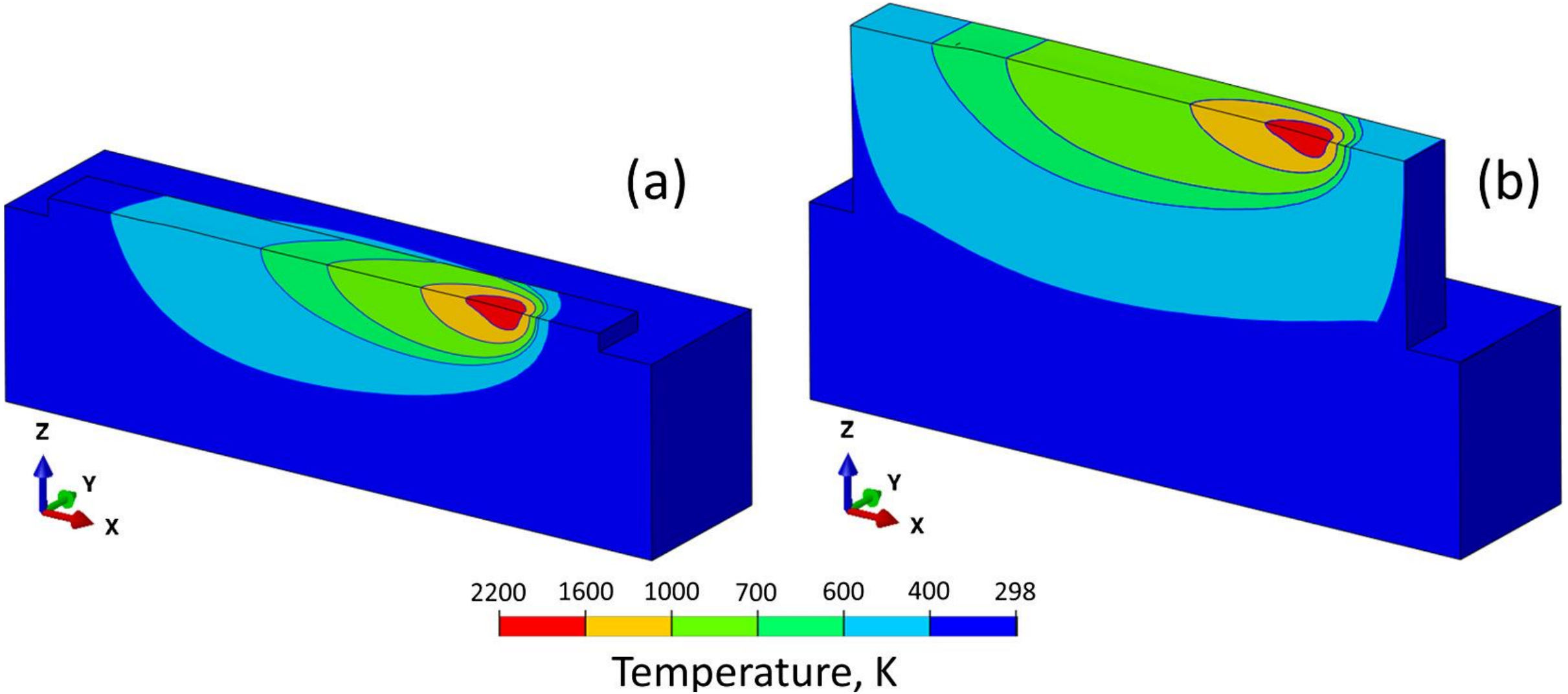

- Fig 7 a e b: computed temperature distribution for the 1st and 10th layers, respectively, during a 10-layerhigh DED-L of IN 718 powder.
- conduction heat loss through the substrate decreases progressively with the deposition of layers. As a result, the peak temperature for the upper layers increases. Because of the rapid scanning of laser beam, the temperature contours are elongated behind the heat source and compressed in front of the beam.

O campo de velocidade do líquido dentro da poça

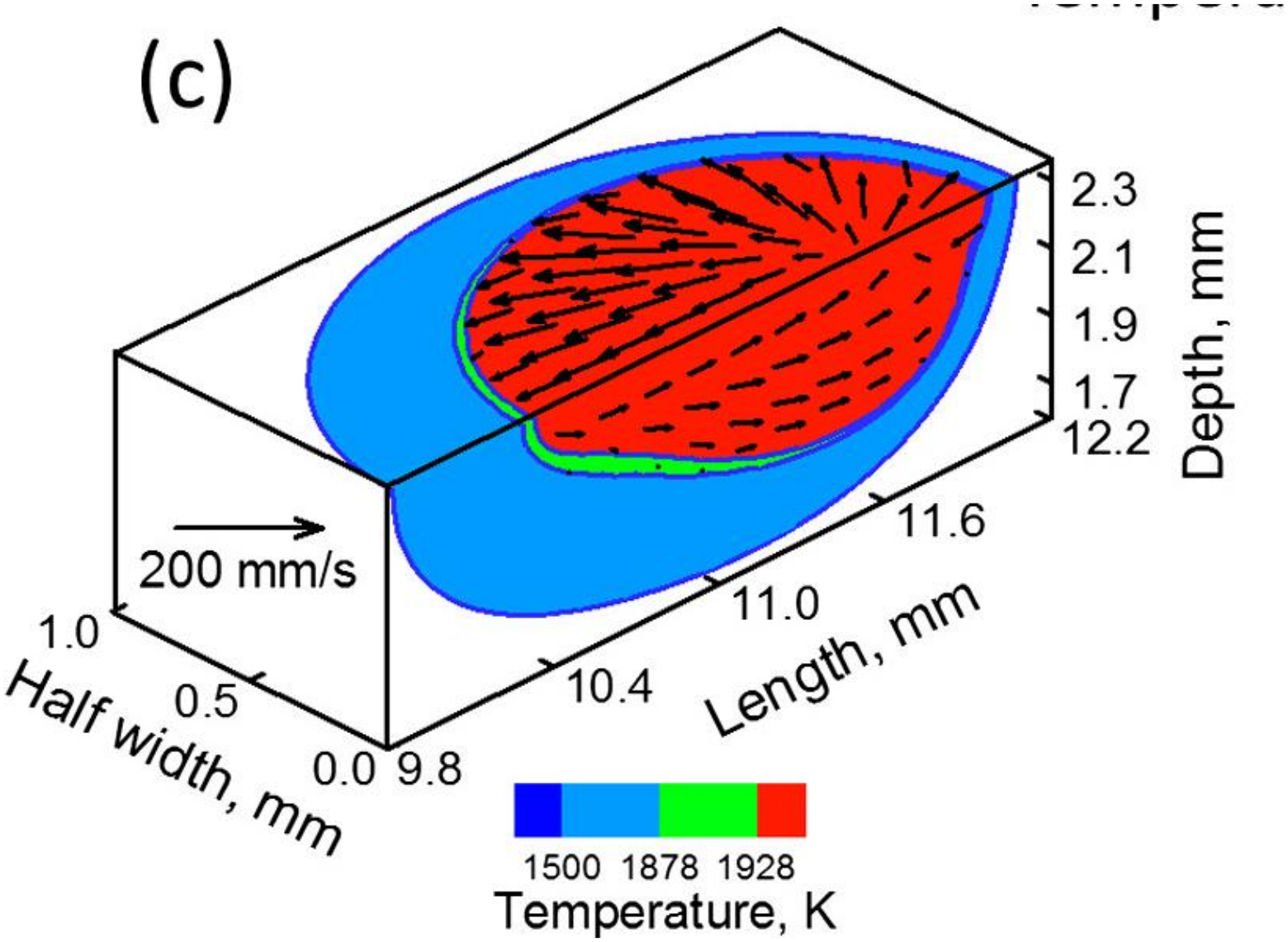

- Fig 7c: The molten pool shape and size at the mid length of the build while depositing the 10th layer.
- The velocities are larger at the surface than in the interior because the motion of the liquid metal in the molten region originates at the surface owing to the Marangoni convection.
- Only one half of the molten pool is presented to show the temperature and velocity fields both on the surface and in the interior on the longitudinal symmetry plane.
- Inside the molten pool, the temperature is the highest near the heat source axis and the lowest near the boundary of the pool.
- This non-uniform temperature results in a surface tension gradient inside the molten pool.

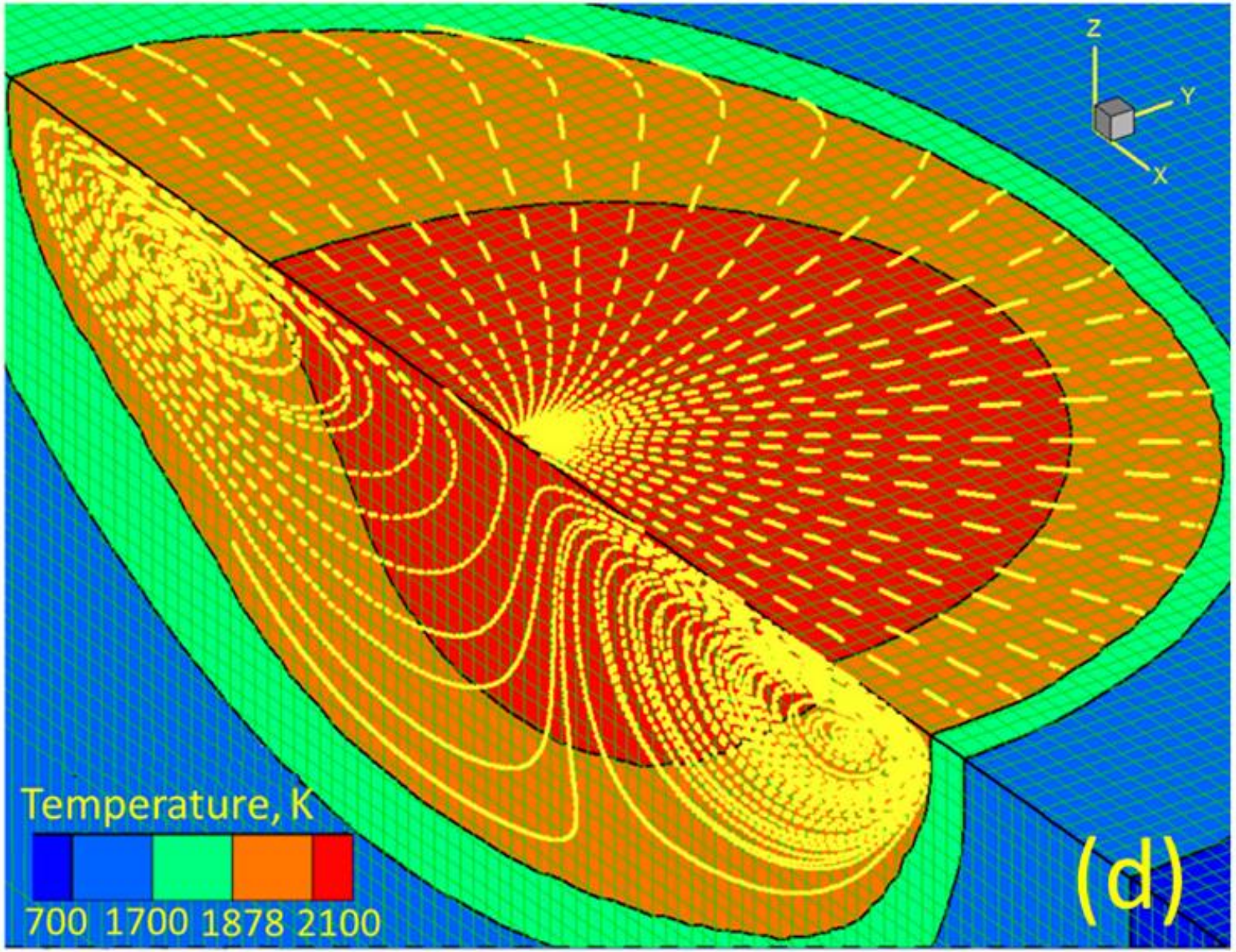

Fig. 7(d) shows that
inside the molten pool the flow of molten metal is driven by the surface tension gradient.

? O que mostra essa figura? Ela não está na referência.

Linhas de isovelocidade?

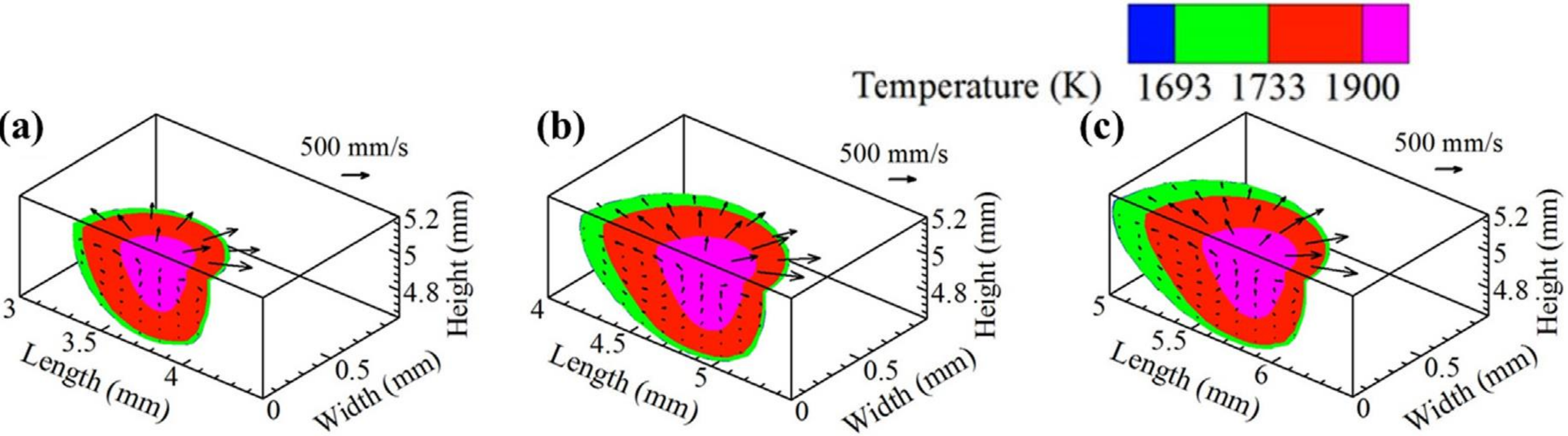

Evolution of the melt pool geometry in the first three layers. (a)–(c) show the progression of deposition in the first layer, (d)–(f) show changes in the melt pool geometry in the second layer, and (g)–(i) show the same in the third layer. **(Legenda da ref 79 é diferente da legenda do artigo)**

The computed motion of liquid metal in the molten pool at the various locations of the build is shown by arrows in Fig. 8 [79]. Since the molten pool moves with the heat source, snapshots of the molten pool at different locations are shown. **Velocities shown by the black arrows range from several hundred mm/s up to about one m/s** depending on the location. Velocities of similar magnitudes were also reported in laser and electron beam welding. The progressive growth of the size of the melt pool in a nine-layer structure is contributed by the spatial variation of the heat transfer rates.

Heat transfer from the molten pool into the substrate becomes more difficult with increasing distance from the substrate. The reduction of heat loss results in larger melt pool and higher peak temperatures in the upper layers.

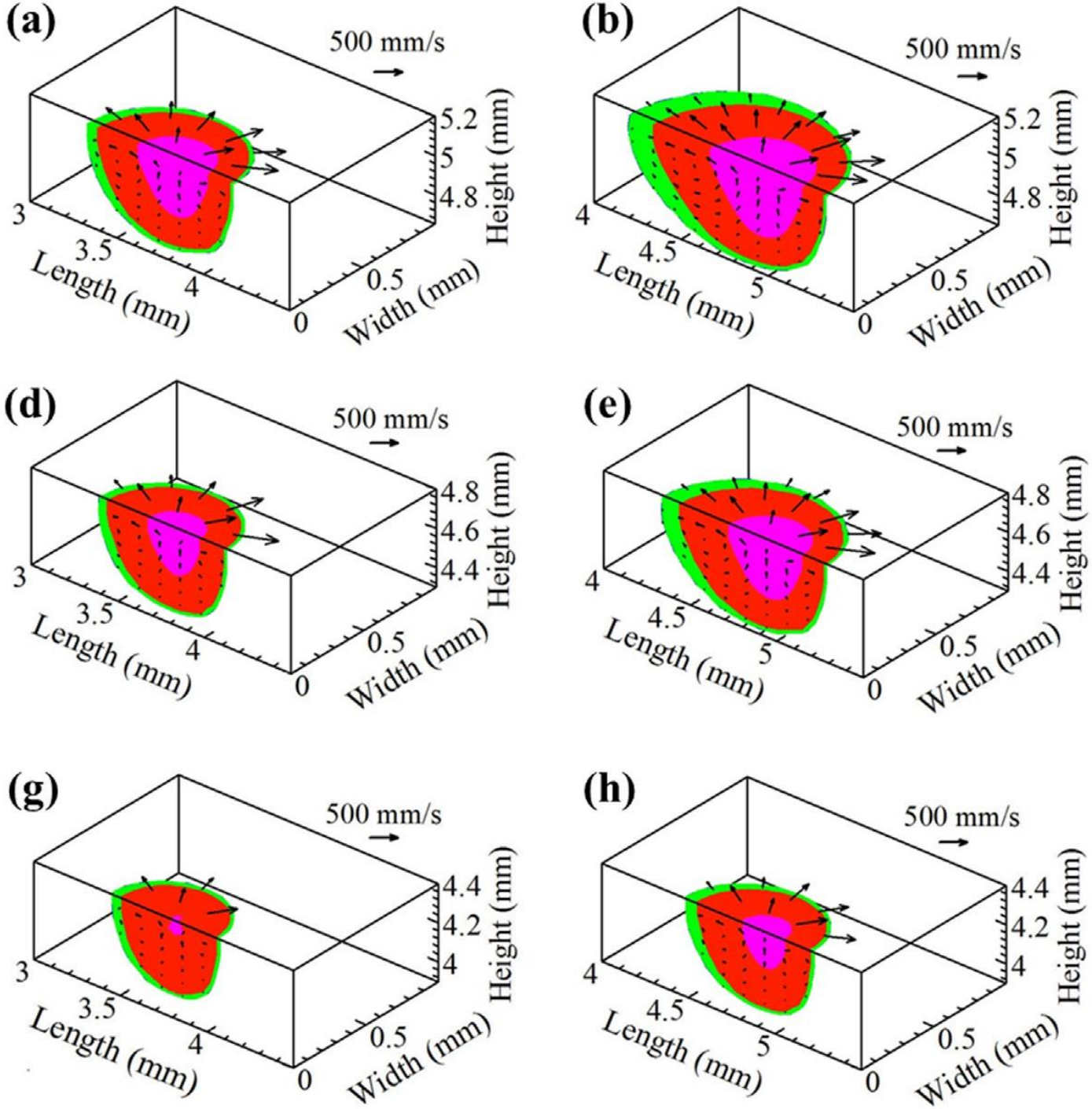

Heat transfer from the molten pool into the substrate becomes more difficult with increasing distance from the substrate. The reduction of heat loss results in larger melt pool and higher peak temperatures in the upper layers.

Evolution of the melt pool geometry in the first three layers. (a)–(c) show the progression of deposition in the first layer, (d)–(f) show changes in the melt pool geometry in the second layer, and (g)–(i) show the same in the third layer. **(Legenda da ref 79; entretanto,a indicação de Height sugere outra coisa.**

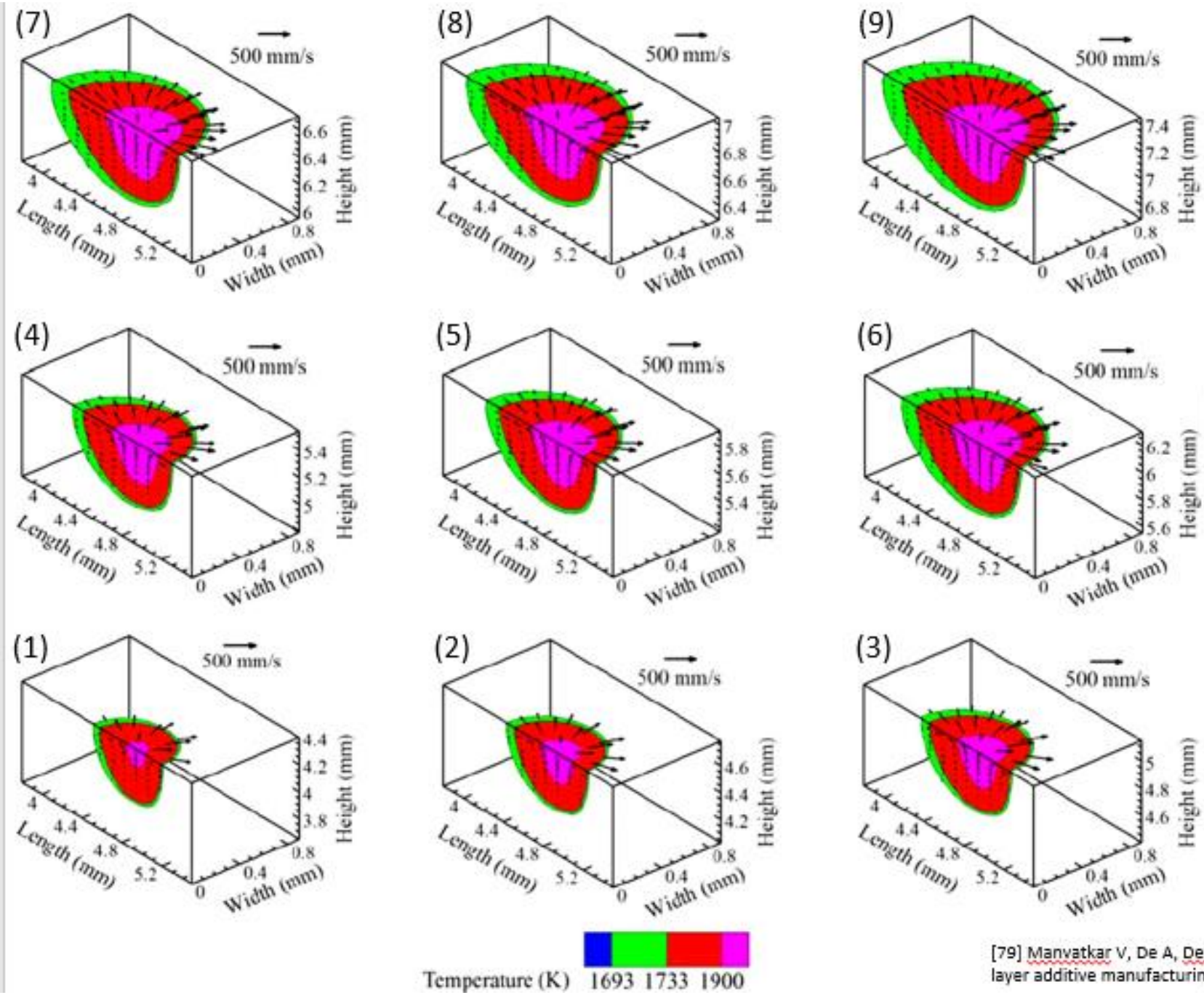

Campos de forma, temperatura e velocidade da poça de fusão da primeira à nona camada, a meio comprimento de deposição. DED-L (210 W) inox. 316, com velocidade de varredura de 12,7 mm/s.

Grato ao prof Willy
Ank de Moraes

[79] Manvatkar V, De A, DebRoy T. Heat transfer and material flow during laser assisted multi-layer additive manufacturing. J Appl Phys 2014;116(12): Article No. 124905.

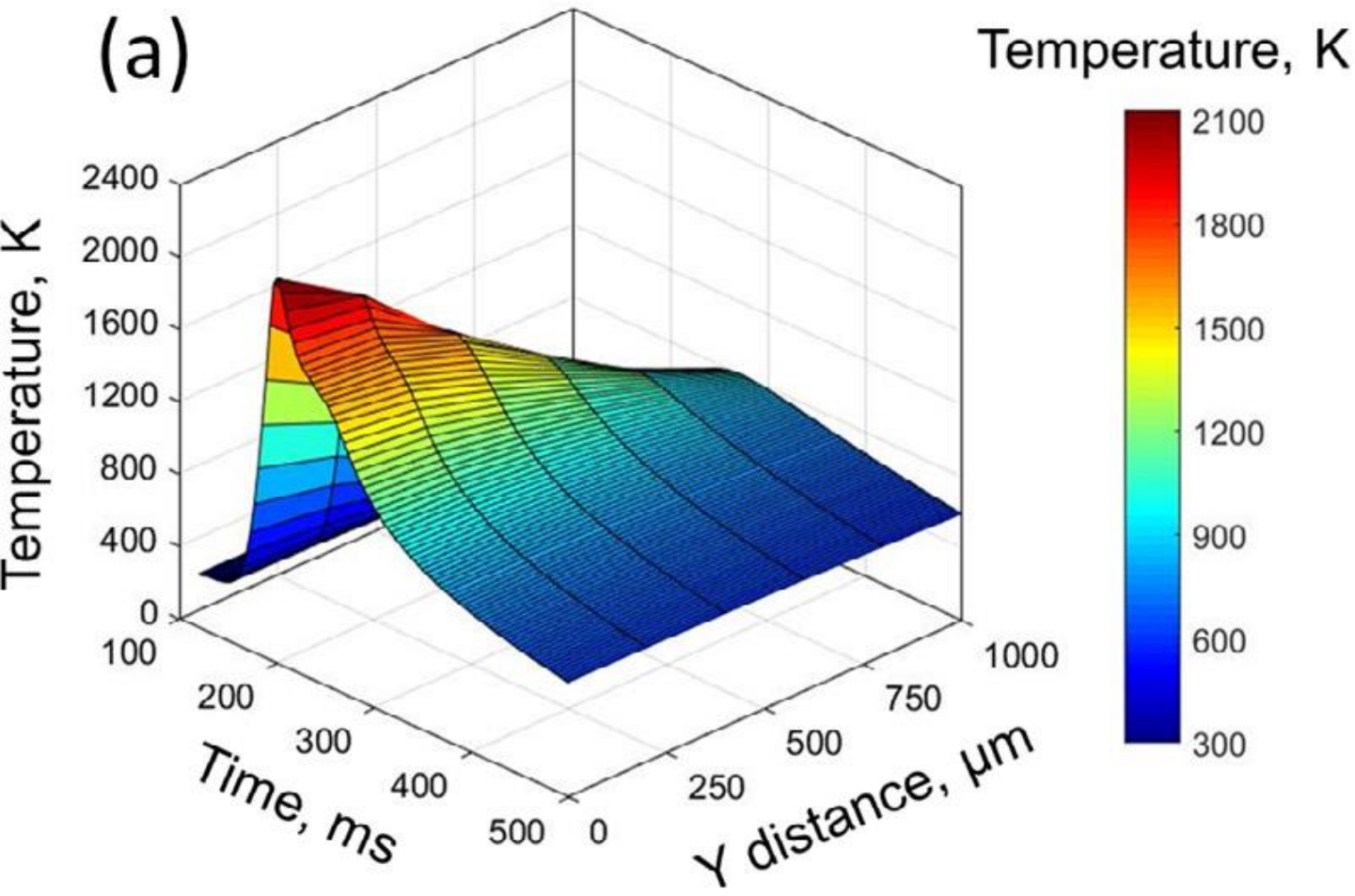

Fig. 9. (a) Temperature variation with time at different locations on the top surface of the deposit during a single layer laser assisted deposition of IN 718 powder on IN 718 substrate using the power of 250W and 15 mm/s scanning speed [141].

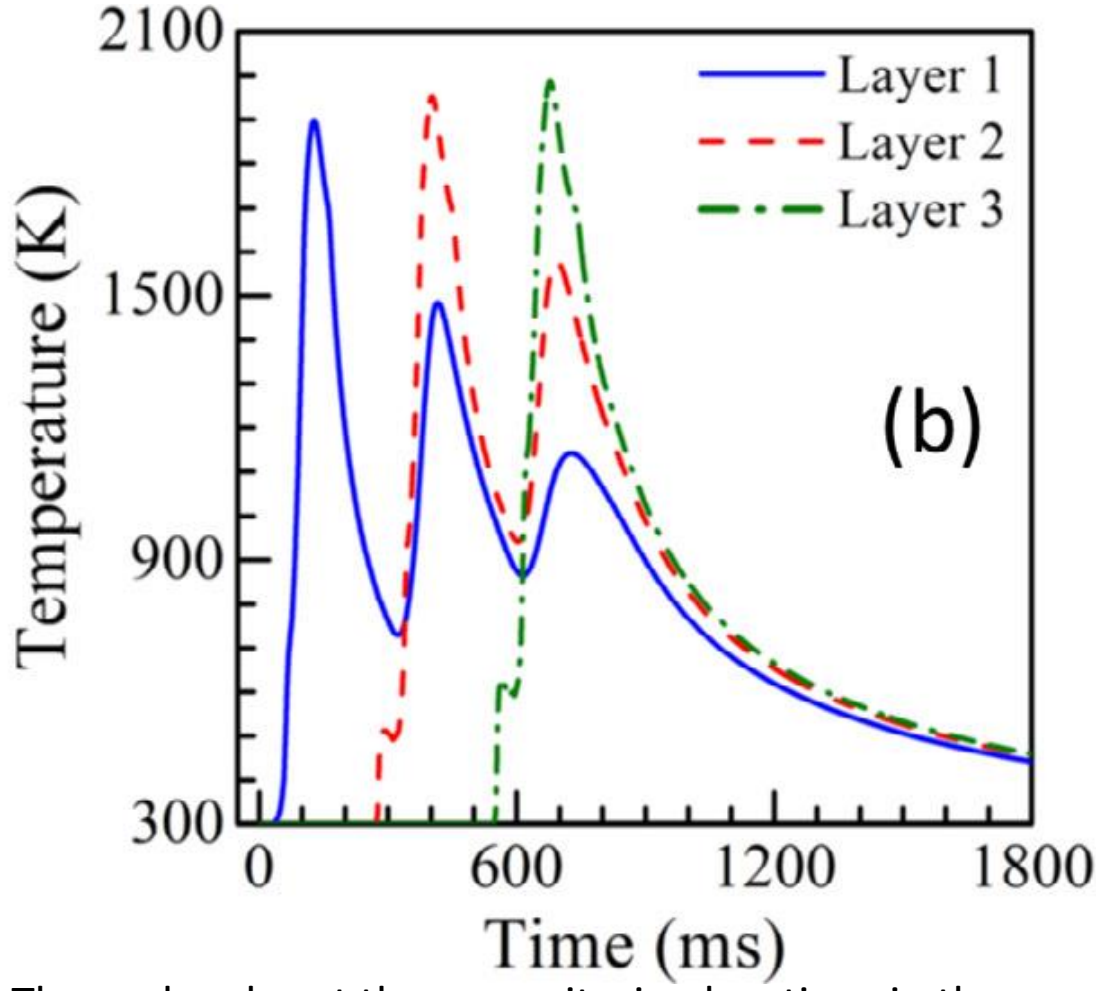

b) Thermal cycles at three monitoring locations in the first three layers in a laser assisted DED of 316 stainless steel at a laser power of 210Wand 12.7 mm/s speed. The monitoring locations are at the mid height and midlength of each layer

A microestrutura da solifidicação

- A taxa de crescimento da frente de solidificação (local solidification growth rate), R, e o gradiente térmico, G, na interface solido-liquid são os mais importantes parâmetros a controlar a **estrutura de solidificação**
- The ratio of the parameters, G/R, affects the morphology of the solidification structure and GR, the cooling rate, affects the **scale of the microstructure.**
- The shape of the fusion zone and the temperature field affect both G and R. The rapid heating and cooling of AM processes leads to sharp peaks in time temperature Plots that result in steep slopes, i.e. high heating and cooling rates.
- Depending on the alloy system and the location of the build where measurements are taken, cooling rates may vary significantly.
- It is important to note that it is meaningless to specify one unique cooling rate value for AM thermal cycles as cooling rate is a strong function of the temperature and location at which it is measured.

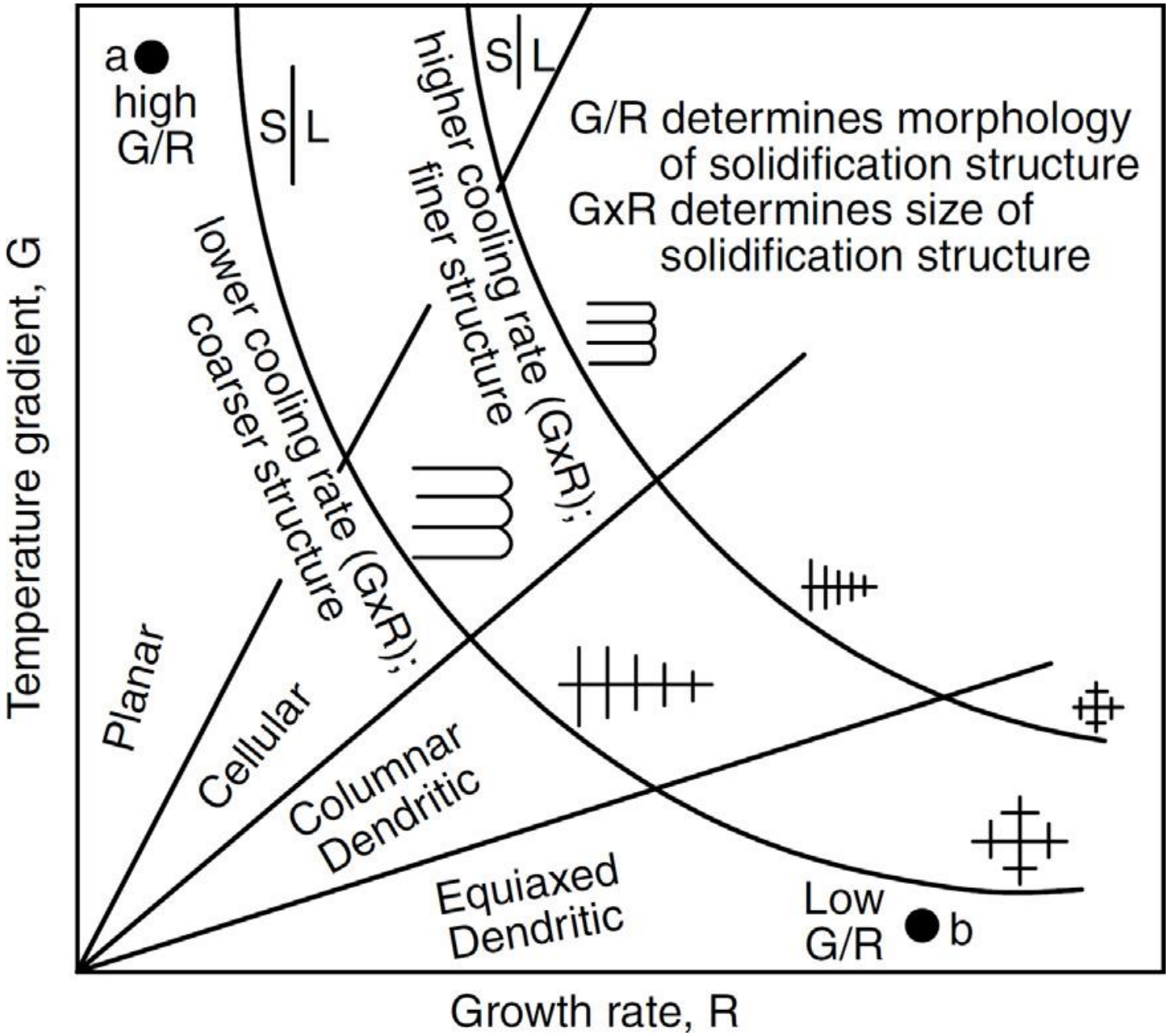

G, R e a microestrutura

- A solidificação mudará de planar para celular, colunar dendrítico ou dendrítico equiaxial , conforme aumenta a taxa de crescimento R.
- Discutiremos isso no item 3.1.3.1

Comparando taxas de resfriamento

Table 6
Comparison of cooling rates of AM with other common manufacturing processes.

Process	Cooling rate [K/s]	Remarks	Ref.
AM cooling rates			
DED-L	3×10^3–7×10^3	SS 316 deposit, speed is 12.7 mm/s	[79]
DED-L	1×10^3–4×10^3	SS 316 deposit, speed is 15 mm/s	[143]
DED-L	5×10^3–3×10^4	IN 718 deposit, speed is 25–40 mm/s	[144]
DED-GMA	10^2–10^3	Ti-6Al-4V deposit, other details are unknown	[145]
PBF-EB	5×10^4	IN 718 deposit, speed is 500 mm/s, 750 °C preheat	[146]
PBF-EB	5×10^4	Ti-6Al-4V deposit, speed is 1500 mm/s, 600 °C preheat	[147]
PBF-L	5×10^5	Ti-6Al-4V deposit, speed is 1000 mm/s	[131]
PBF-L	1×10^6–6×10^6	Al alloy deposit, speed is 100–400 mm/s	[148]
Common manufacturing processes			
Casting	10^0–10^2		[142]
Arc welding	10^1–10^3		
E-beam welding	10^2–10^4		
Laser welding	10^2–10^6		

Note: The cooling rates are either specified in the literature or approximately estimated from the thermal cycle provided. All cooling rates specified here are measured or calculated between the liquidus and the solidus temperatures of the corresponding alloy at a location directly below the central axis of the heat source.

Faixas de temperatura relevantes para saber taxa de resfriamento

- Entre Tliquidus e T sólidus
- Para aços, taxa entre 800e 500oC
- Para ligas Ti, taxa abaixo da Beta Transus afeta microestrutura de alfa + beta.

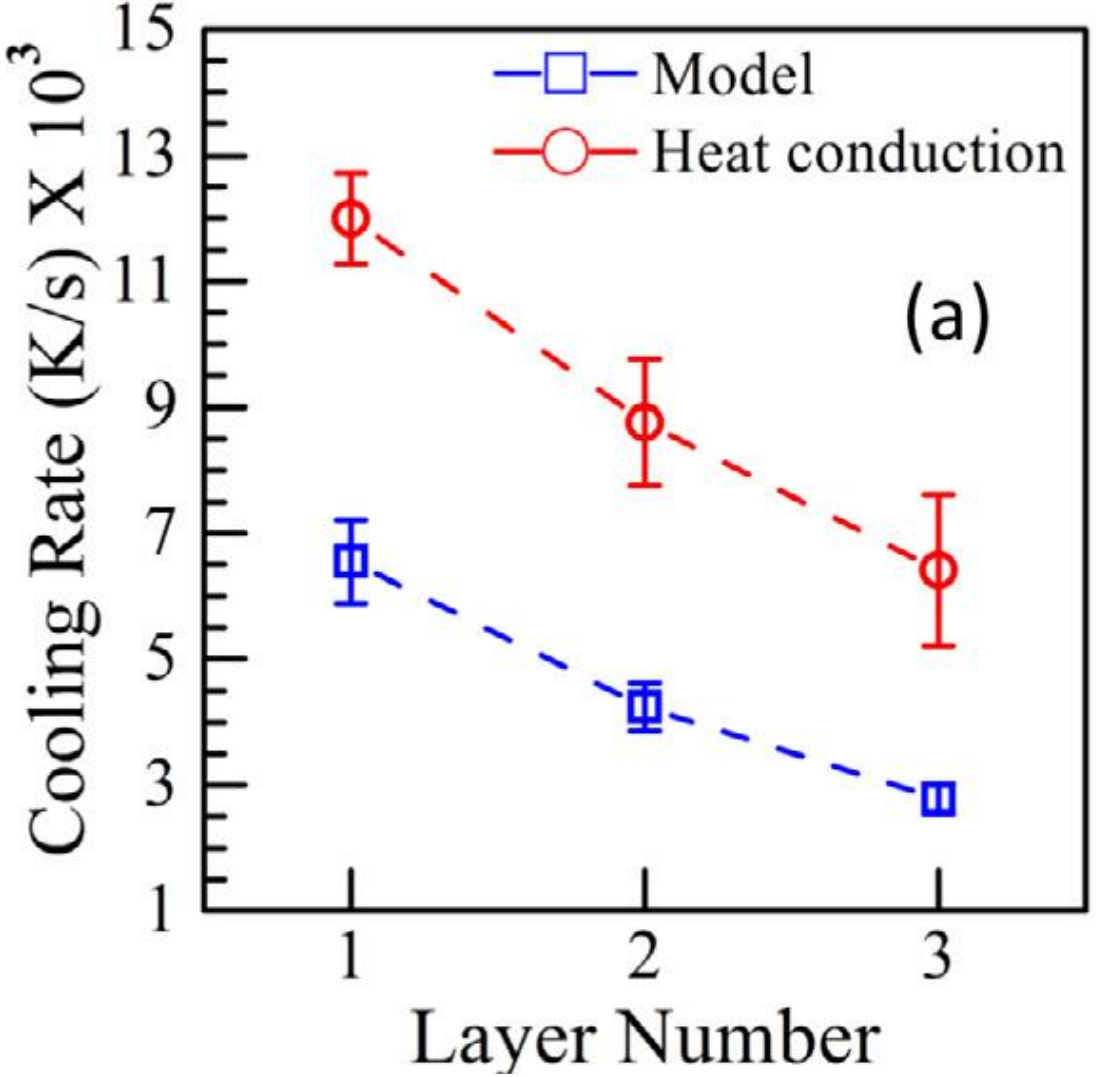

Fig. 10. (a) Variation of cooling rate between peak temperature and liquidus temperature

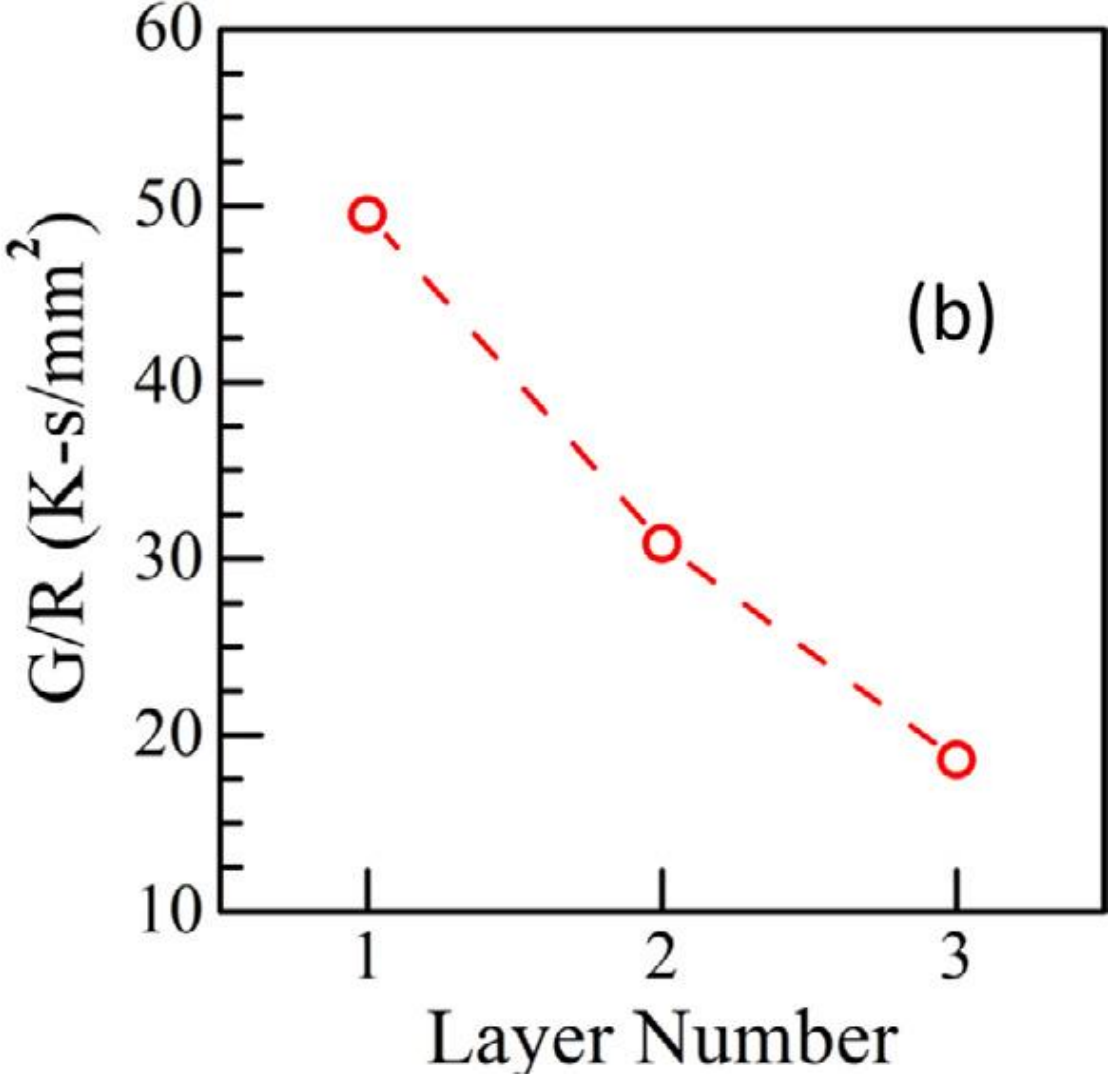

G/R ratio at three monitoring locations in the three layers

in a laser assisted DED of 316 stainless steel at a laser power of 210W and 12.7 mm/s speed [79].

These variations result in inhomogeneous microstructures and properties in different regions of a part. At each location within a part, the microstructure and the grain structure of the alloy that forms after the first thermal cycle is often changed by the subsequent thermal cycles. Reliable transient 3D temperature fields are thus a prerequisite.

2.7. Números adimensionais

- Nondimensional numbers are beneficial because they reduce the total numbers of variables to be studied and provide important understanding that a single process variable is unable to provide [143].
- Their effectiveness for providing insight about the AM process originates from the fact that very often a group of variables, rather than a single variable, affect the performance and outcome of a complex process such as AM.

- The relative importance of heat transfer by convection and conduction in the molten pool in AM can be determined from the Peclet number, Pe:

$$Pe = \frac{UL}{\alpha}$$

$$\alpha = \frac{k}{\rho c_p}$$ [4] (m²/s)

where

- k is thermal conductivity (W/(m·K))
- c_p is specific heat capacity (J/(kg·K))
- ρ is density (kg/m³)

- U is the characteristic velocity,
- α is the thermal diffusivity of the alloy
- and L is the characteristic length, generally considered as pool length.
- A high value of Peclet number (Pe>>1) indicates that convective heat transfer is the main mechanism of heat transfer within the molten pool.

Relembrando difusividade térmica

Na análise de transferência de calor, **difusividade térmica** é a condutividade térmica dividida por densidade e capacidade específica de calor a pressão constante.[1] Mede a taxa de transferência de calor de um material do lado quente para o lado frio. Ele tem a unidade derivada SI de m² / s. A difusividade térmica é geralmente denotada *α* mas *a*, *κ*,[2] *K*,[3] e *D* também são usados. A fórmula is:

$$\alpha = \frac{k}{\rho c_p}$$ [4]

onde

- k é condutividade termal (W/(m·K))
- ρ é densidade (kg/m³)
- c_p é capacidade de calor específica (J/(kg·K))

Juntos, ρc_p podem ser considerados a capacidade de calor volumétrico (J/(m³·K)).

Número de Marangoni

$$Ma = -\frac{d\gamma}{dT}\frac{L\Delta T}{\mu\alpha}$$

- where μ is the viscosity, α is the thermal diffusivity of the alloy,
- L is the characteristic length of the molten pool, which is taken as the width of the molten pool,
- ΔT is the difference between the maximum temperature inside the pool and the solidus temperature of an alloy,
- and dγ/ dT is the sensitivity of surface tension with respect to temperature.
- The shape and size of the deposit depends on the convective flow of the molten metal inside the pool driven by the surface tension gradient in the pool.
- Marangoni number represents the ratio of the surface tension force to viscous force and is a measure of the strength of the convective flow of liquid metal within the molten pool.

Número de Fourier

- Fourier number (Fo) is used to obtain a relative measure of heat dissipation rate to heat storage rate during AM processing.

$$F_o = \alpha\tau / L^2$$

- where α, τ and L refer to thermal diffusivity, characteristic time scale and length, respectively.
- The characteristic time can be expressed as L/v, where L and v are the pool length and scanning speed respectively [135]. So, Eq. (10) can be re-written as,

$$F_o = \alpha / vL$$

- Higher Fo means faster dissipation of heat which helps in faster cooling of the build and more refined microstructure

Sensibilidade à distorção térmica ε*

- A non-dimensional thermal strain parameter (ε*) represents the effects of common process parameters and material properties on the susceptibility of a component to thermal distortion

$$\varepsilon^* = \frac{\beta \Delta T}{EI} \frac{tH^{3/2}}{F_o \sqrt{\rho}}$$

- where β is the volumetric coefficient of thermal expansion,
- ΔT is the maximum rise in temperature during the process,
- E is the elastic modulus
- I is the moment of inertia of the substrate, the product, EI, is the flexural rigidity of the structure,
- t is the characteristic time,
- H is the heat input per unit length, Fo is the Fourier number and ρ is the density of the alloy powder.

Adimensional de entrada de calor Q^*

$$Q^* = (P/v)/(P_R/v_R)$$

A non-dimensional heat input (Q^*) is used as a measure of the energy deposited per unit length of the deposit.

where P and v refer to the laser power and the scanning speed,
P_R and v_R represent the reference laser power and scanning speed, respectively.

Higher heat input per unit length reduces cooling rate and makes the microstructure coarser.
For most alloys the hardness decreases with higher heat input.

Efeitos do Heat Input

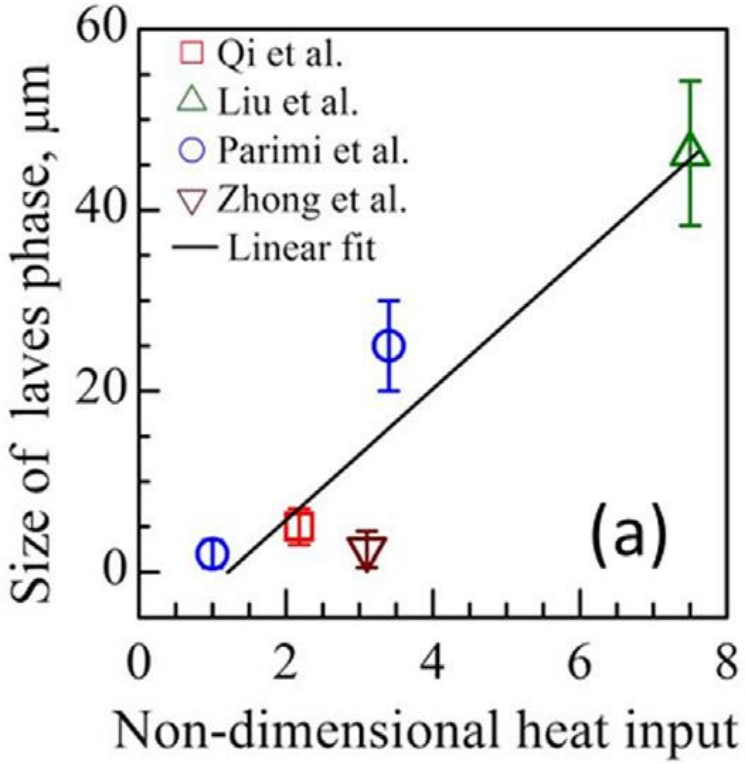

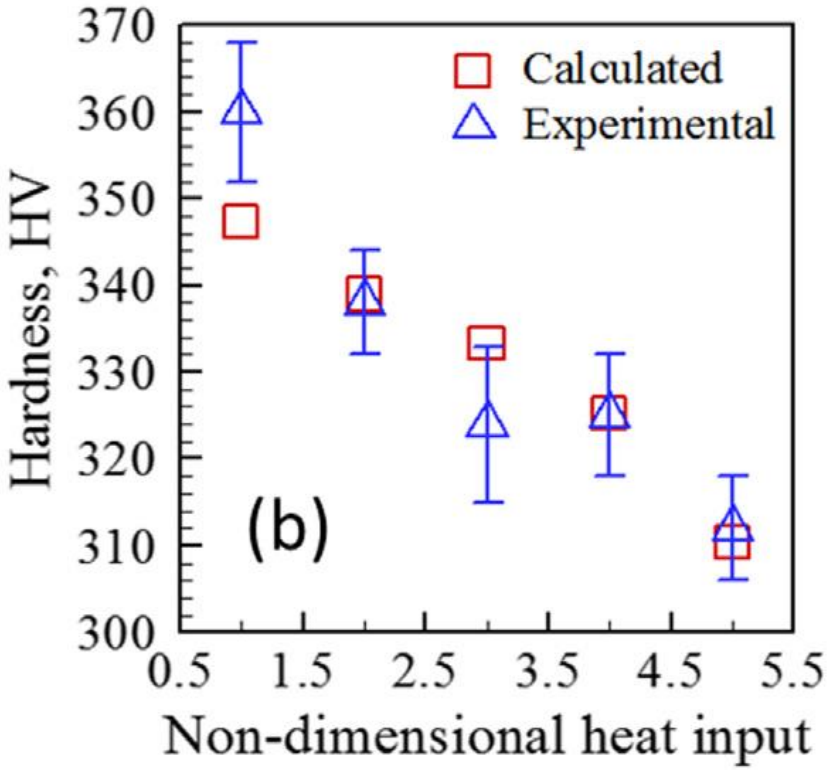

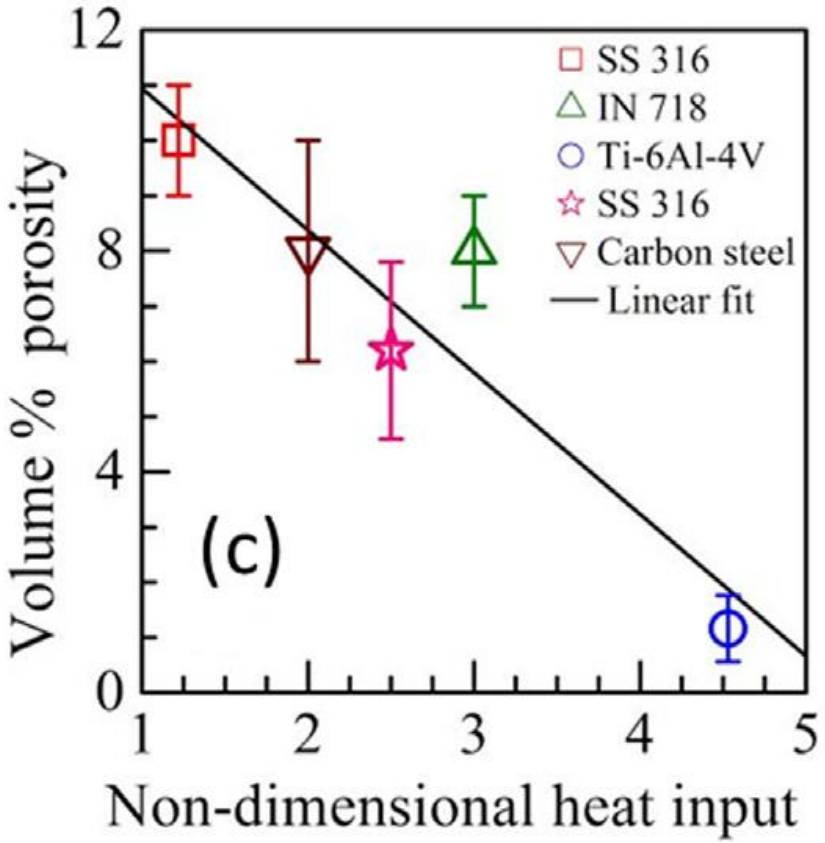

Significados de alguns Adimensionais

Table 7
Important non-dimensional numbers and their significance [143,151].

ND numbers	Significance
Non-dimensional heat input (Q^*)	• Represents the relative magnitude of linear heat input • Higher non-dimensional heat input results in higher peak temperature and pool dimensions and slow cooling
Marangoni number (Ma)	• Signifies the convective flow of the molten metal inside the pool driven by surface tension gradient • Higher Marangoni number results in larger pool with high aspect ratio, which in turn, help ensures proper interlayer bonding and hence low porosity
Peclet number (Pe)	• Indicates the relative importance of convective heat transfer over heat transfer by conduction • If Pe > 1, convective heat transfer is dominant
Fourier number (F_o)	• Represents the ratio of heat dissipation rate to heat storage rate • Higher Fourier number indicates high rate of heat dissipation hence faster cooling • Higher Fourier number results in low heat storage hence low thermal distortion
Strain parameter (ε^*)	• Embodies all important process parameters and alloy properties that affect the thermal strain and distortion • Linearly correlated with thermal strain during AM • Does not consider the plastic strain generated during the fabrication

2.8. Estabilidade dos Processos

- Rapid production of AM parts is often achieved by increasing the scanning speed. As a result, the molten pool becomes elongated and depending on the scanning speed, the liquid pool may become unstable as evidenced by break-up of the single molten pool into isolated puddles of liquid resulting in a discontinuity of the deposited geometry and non-uniform deposit thickness.
- The origin of the defects is often caused by
  - the Kelvin-Helmholtz hydrodynamic instability or
  - the Plateau Raleigh capillary instability.

2.8.1. A instabilidade hidrodinâmica de Kelvin Helmholtz

- Um defeito, tanto na soldagem como no DED-arco, é conhecido como “humping”, quando o cordão de solda fica descontínuo.
- Esse defeito é causado por uma instabilidade da poça líquida, chamada de instabilidade de Kelvin Helmholtz, associada com a diferença de velocidade entre a do gas e a do líquido na poça.
- O defeito ocorre quando o adimensional de Richardson é menor que 0,25

$$Ri = \frac{gL}{(U_g - U_l)^2}$$

g é a aceleração da gravidade
L é a espessura da camada dividido por 2
Ug e Ul são a velocidade do gás de proteção e a velocidade do líquido
A velocidade do líquido depende das variáveis do processo.

“Humping” num cordão de solda

Hump = corcova

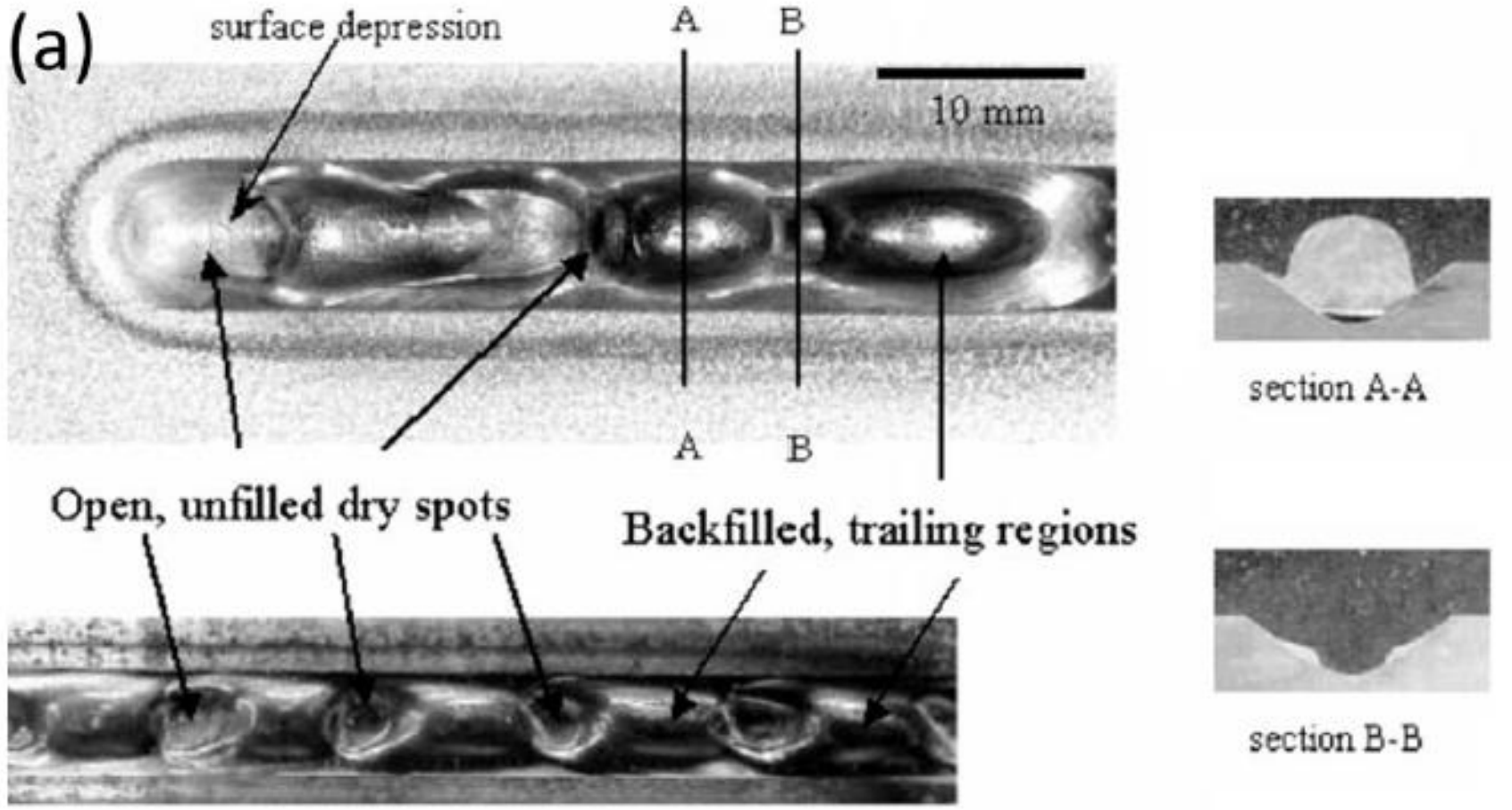

The front of the molten pool exhibits a large depression known as the gouging region.
The trailing region, consisting of bulk of the molten metal resides in the back of the melt pool.
The wavelength of the humping beads was calculated by solving the wave propagation equation on the molten pool surface for various welding parameters

Gouge=cava

“humping” na M.A. : o efeito da velocidade de varredura no DED-GMA

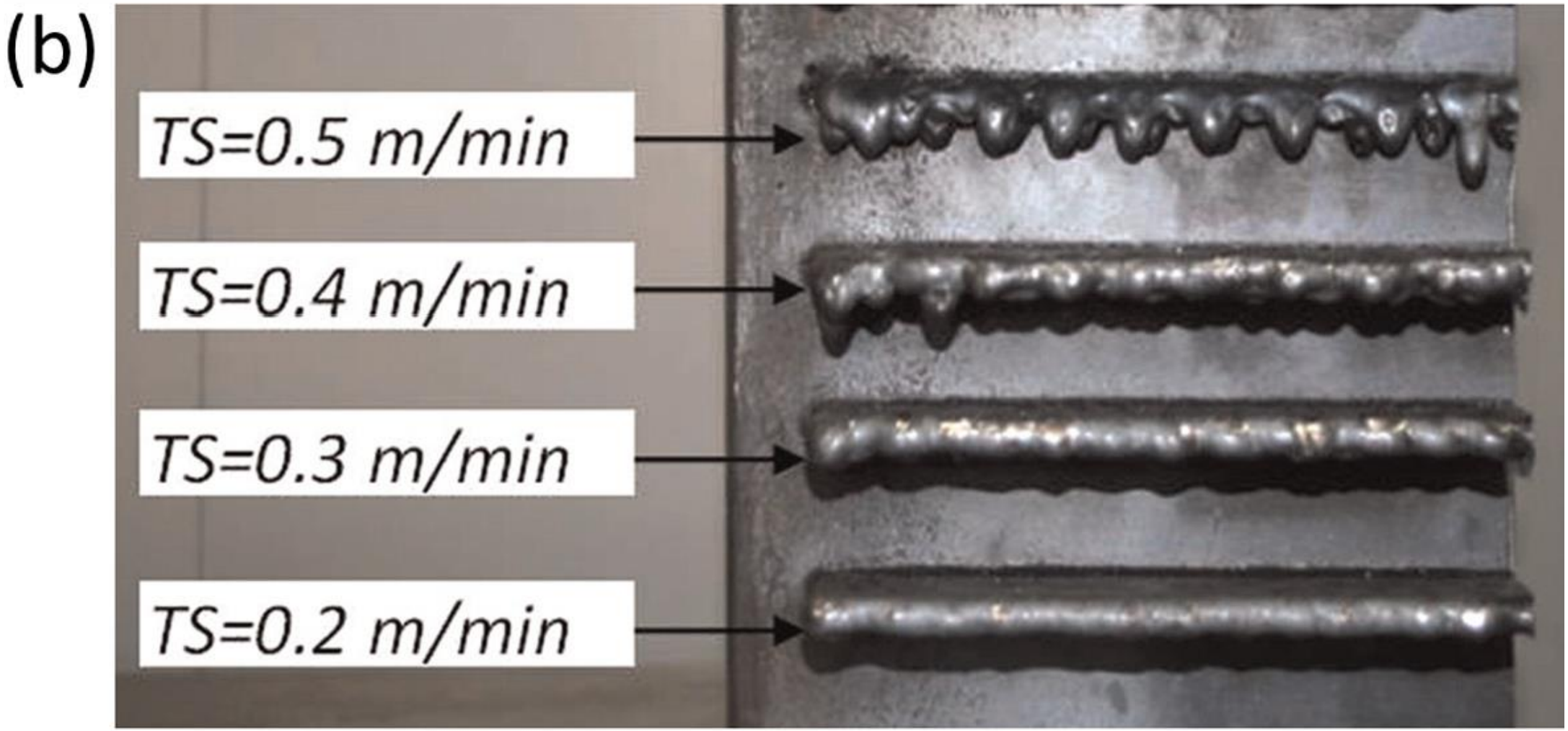

Observou-se Humping em DED-GMA, DED-PA, and DED-L.

humping tends to occur when the scanning speed exceeds a certain critical value, mas deve depender de power, speed, layer thickness, hatch spacing and feed rate.

2.8.2. Instabilidade capilar do Plateau Raleigh e o “Balling”

- “Balling” é um defeito comum.
- A trilha, que teria uma forma cilíndrica, pode apresentar variaçõe de diâmetro e até separar-se em gotas.

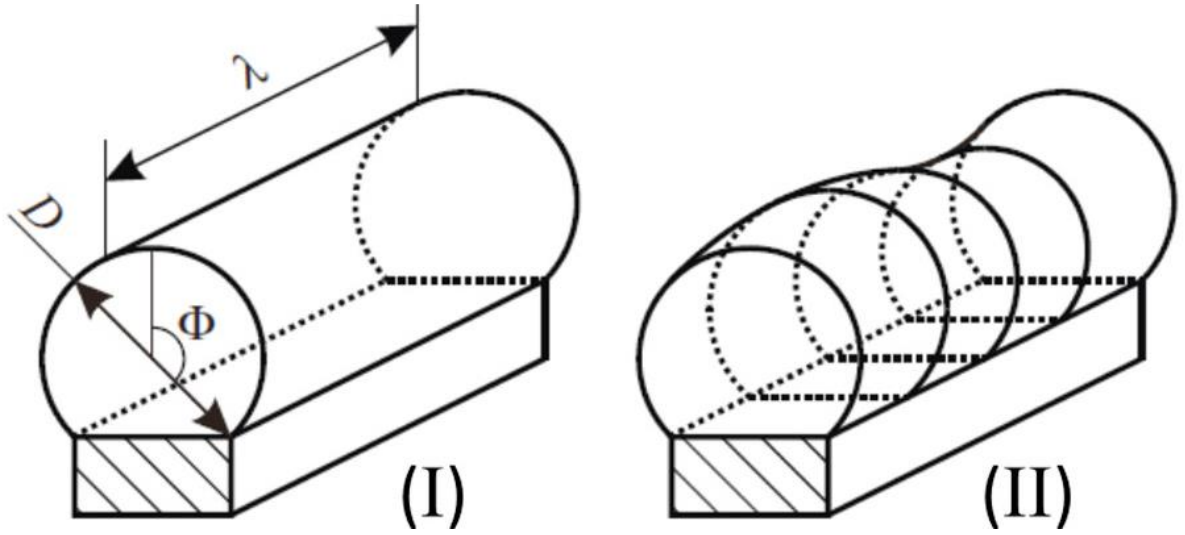

- The maximum allowable length of the molten pool that prevents this instability can be obtained from the following relation based on Plateau Raleigh capillary instability.

$$L/D \geqslant \pi$$

L é o comprimento da poça e D é a largura do depósito.

Balling em PBF-L
(será melhor discutido em 2.9.1)

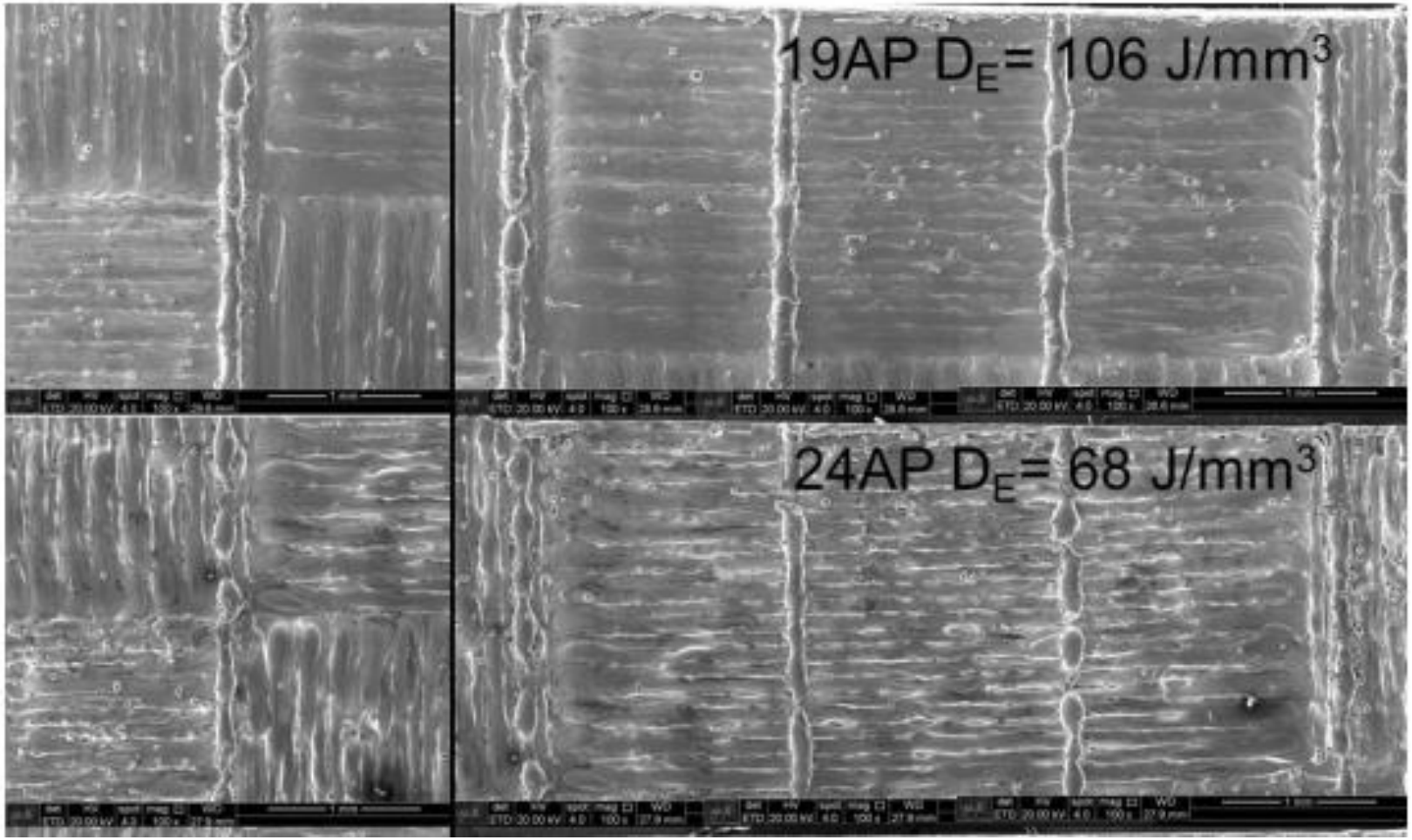

- P=300W
- V=900 mm/s

- V=1400 mm/s

Aumento de v
Causa “balling”

Jhoan Guzman, 2019, diss. de mestrado, USP

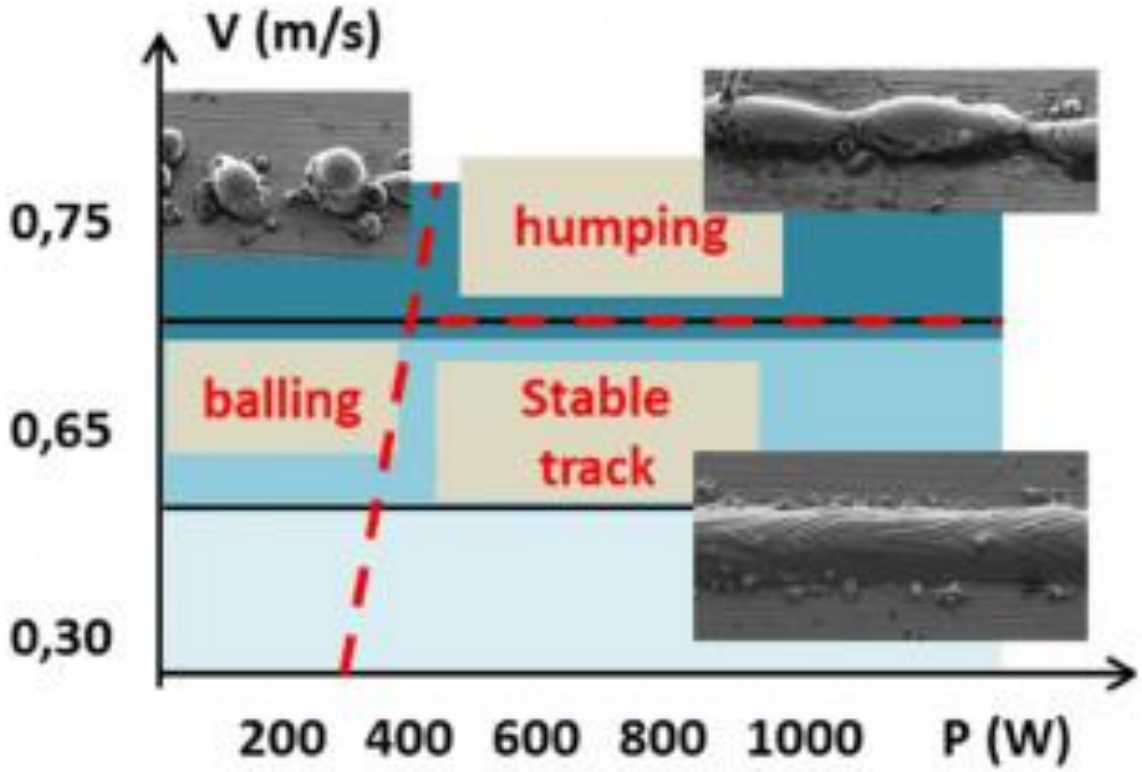

FIG. 21. LPBF process map indicating the zones of instabilities.

Valérie Gunenthiram, Patrice Peyre, Matthieu Schneider, Morgan Dal, Frédéric Coste, Rémy Fabbro. **Analysis of laser–melt pool–powder bed interaction during the selective laser melting of a stainless steel**

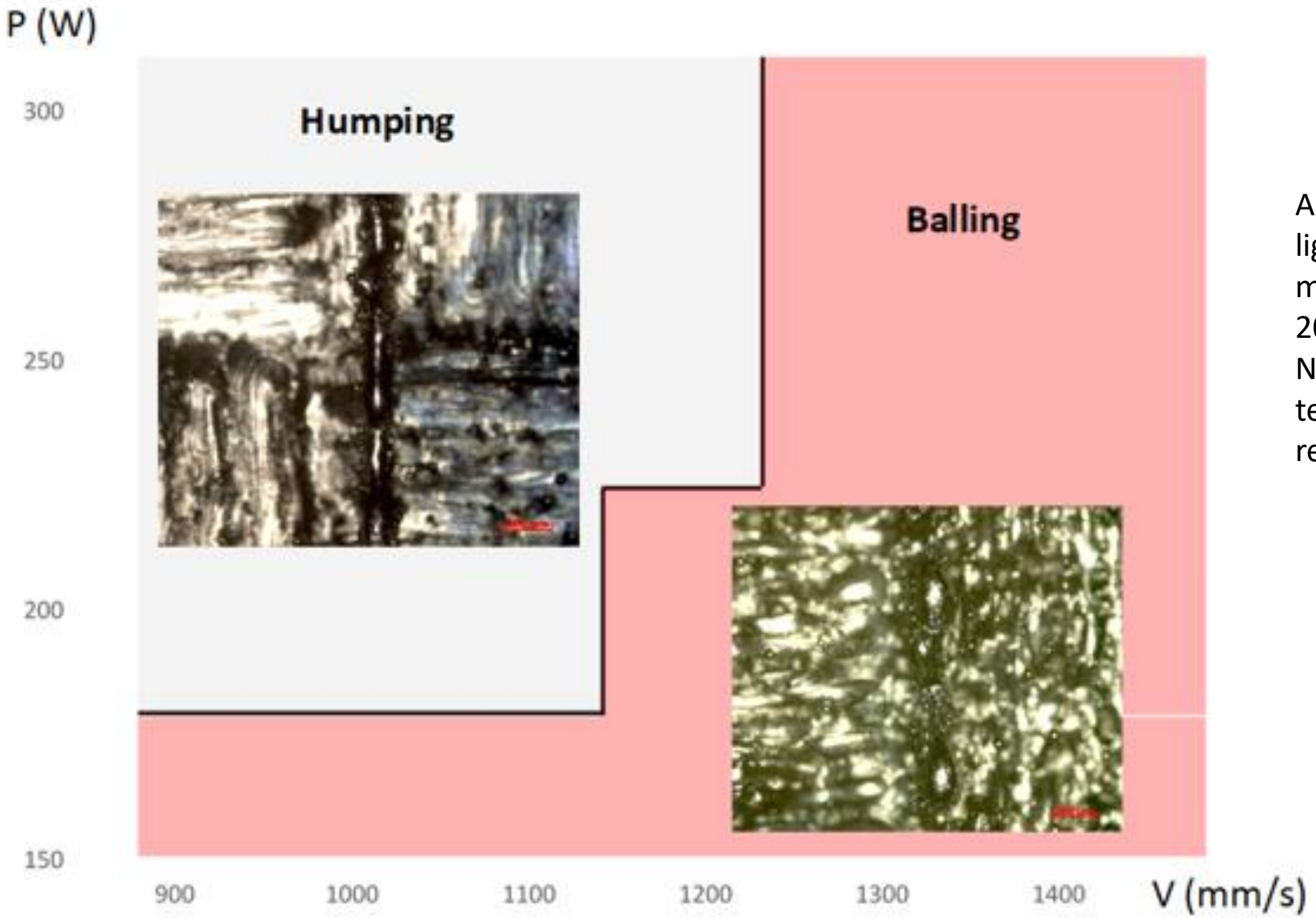

Análise das trilhas isoladas em ligas TiNb investigadas em mestrado de Jhoan Guzman, 2019, EPUSP.
Nenhuma das condições testadas nesse retângulo resultou em trilha estável

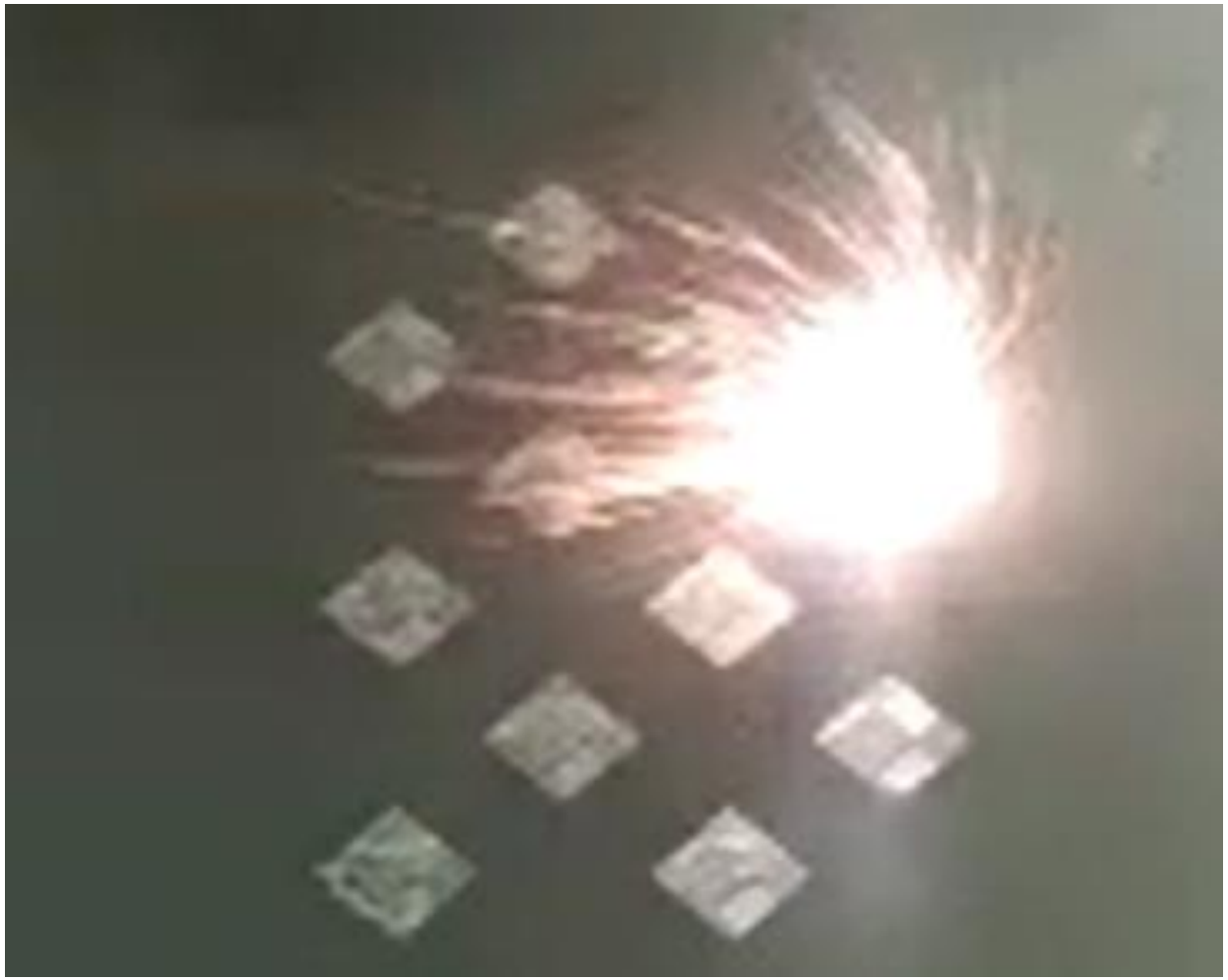

O efeito da direção do vento:

O gás de proteção é soprado da esquerda para a direita.